# Differential cross sections for the electron impact excitation of the $A\,^3\Sigma_u^+$, $B\,^3\Pi_g$, $W\,^3\Delta_u$, $B'\,^3\Sigma_u^-$, $a'\,^1\Sigma_u^-$, $a\,^1\Pi_g$, $w\,^1\Delta_u$, and $C\,^3\Pi_u$ states of $N_2$

M. A. Khakoo,[1] P. V. Johnson,[2] I. Ozkay,[1] P. Yan,[3] S. Trajmar,[2] and I. Kanik[2]
[1]*Department of Physics, California State University, Fullerton, California 92834, USA*
[2]*Jet Propulsion Laboratory, California Institute of Technology, Pasadena, California 91109, USA*
[3]*Troy High School, Dorothy Lane, Fullerton, California 92831, USA*
(Received 10 February 2005; published 13 June 2005)

Measurements of differential cross sections for the electron-impact excitation of molecular nitrogen from the ground $X\,^1\Sigma_g^+(v''=0)$ level to the $A\,^3\Sigma_u^+(v')$, $B\,^3\Pi_g(v')$, $W\,^3\Delta_u(v')$, $B'\,^3\Sigma_u^-(v')$, $a'\,^1\Sigma_u^-(v')$, $a\,^1\Pi_g(v')$, $w\,^1\Delta_u(v')$, and $C\,^3\Pi_u(v')$ levels are presented. The data are obtained at the incident energies of 10, 12.5, 15, 17.5, 20, 30, 50, and 100 eV over the angular range of 5°–130° in 5° intervals. The individual electronic state excitation differential cross sections are obtained by unfolding electron energy-loss spectra of molecular nitrogen using available semiempirical Frank-Condon factors. The data are compared to previous measurements and to available theory. We also make several important suggestions regarding future work that, like the present, relies on the unfolding of electron energy-loss spectra for obtaining differential cross sections.

DOI: 10.1103/PhysRevA.71.062703 PACS number(s): 34.80.Gs, 34.50.Gb

## I. INTRODUCTION

$N_2$ is one of the most studied molecules with respect to electronic excitation by electron impact. This is due to the importance of electron-$N_2$ scattering (excitation) in the production of aurora and upper atmospheric phenomena of the Earth as well as the planetary atmospheres of the outer planets of our solar system. For recent surveys of electron-impact excitation of $N_2$ see Refs. [1–4], and most recently the excellent review of Brunger and Buckman [5]. In terms of differential electron scattering, the available (fragmentary) differential cross-section (DCS) data are in the low to intermediate incident energy region (10–100 eV) at scattering angles from 10° up to ≈140° or at high incident electron energies (above 100 eV) at small scattering angles. For many practical applications as well as for testing low-energy close-coupling theoretical models and approximations, low-energy cross sections are the most needed, while at intermediate and high incident energies, perturbative methods can be tested. While such absolute DCS measurements are made difficult because of the inherent dependence on spectral unfolding routines, it is important to obtain reliability for such measurements to promote theoretical investigations of electron collisions with $N_2$. Unfortunately, the fragmentary data available claim to be accurate to about 25%, but differ from each in many cases by a factor of 2 or more. To a considerable extent, such disagreements have hampered the development of reliable theoretical models. Consequently, there is a great motivation to produce an accurate set of experimental data to facilitate the development of accurate theoretical models.

Experimental investigations and theoretical modeling of the excitation of $N_2$ from its ground state $X\,^1\Sigma_g^+(v''=0)$ state are complicated by several factors. First, the ground state is characterized by a triple bond potential, which is very steep and strongly anharmonic. Consequently, numerical descriptions of its vibrational wave functions will be very sensitive to small displacements of the potential-energy curves along the internuclear axis. This means that theoretical computations of Franck-Condon (FC) factors, which rely on extremely accurate potential curve models, can be expected to be somewhat more difficult to obtain for $N_2$ to the same degree of accuracy as they could be obtained for $H_2$ (which were calculated in a similar electron-scattering project by our group; see Ref. [6]). Second, in terms of molecular orbitals, the $N_2[(1s\sigma_g)^2(1s\sigma_u)^2(2s\sigma_g)^2(2s\sigma_u)^2](2p\pi_u)^4(2p\sigma_g)^2$ ground-state configuration's outer 6-$p$ electrons (outside the brackets =[$KK$] or [closed $K$ shell], see, e.g., Ref. [7], Table 34). These electrons which form the triple bond make for a complicated picture involving significant electron-electron correlation between them. Such electron-electron correlation will challenge simplified models of the excitation of $N_2$ for even the lowest excited states. Tables I and II show the electron configuration, FC factors, and excitation energies of the lowest eight excited states of $N_2$ which lie in the energy-loss region from 6.2 to 11.3 eV, as listed by Lofthus and Krupenie [8]. Clearly, all these listed excitations are dipole-forbidden from the ground state; even the (only) dipole-allowed orbital

TABLE I. Electron configurations for the ground state and the first eight excited states of $N_2$ (from Lofthus and Krupenie [8] and Herzberg [7]). The numbers in italics indicate the excited orbitals.

| | Electron configuration | | | |
|---|---|---|---|---|
| State | $2s\sigma_u$ | $2p\pi_u$ | $3s\sigma_g$ | $2p\pi_g$ |
| $X\,^1\Sigma_g^+$ | 2 | 4 | 2 | |
| $A\,^3\Sigma_u^+$ | 2 | *3* | 2 | *1* |
| $W\,^3\Delta_u$ | 2 | 4 | *1* | *1* |
| $B\,^3\Pi_g$ | 2 | 4 | *1* | *1* |
| $B'\,^3\Sigma_u^-$ | 2 | *3* | 2 | *1* |
| $a'\,^1\Sigma_u^-$ | 2 | *3* | 2 | *1* |
| $a\,^1\Pi_g$ | 2 | 4 | *1* | *1* |
| $C\,^3\Pi_u$ | *1* | 4 | 2 | *1* |
| $w\,^1\Delta_u$ | 2 | *3* | 2 | *1* |

 

TABLE II. Transition energy loss values and FC factors for excitation of $N_2$ from the $X\,^1\Sigma_g^+(v''=0)$ ground state used in the unfolding analysis of the $N_2$ energy loss spectra. See text for details.

| | $A\,^3\Sigma_u^+$ | | $W\,^3\Delta_u$ | | $B\,^3\Pi_g$ | | $B'\,^3\Sigma_u^-$ | | $a'\,^1\Sigma_\mu^-$ | | $a\,^1\Pi_g$ | | $w\,^1\Delta_u$ | | $C\,^3\Pi_u$ | |
|---|---|---|---|---|---|---|---|---|---|---|---|---|---|---|---|---|
| $v'$ | FC | $E_{v''=0,v'}$ | FC | $E_{v''=0,v'}$ | FC | $E_{v''=0,v'}$ | FC | $E_{v''=0,v'}$ | FC | $E_{v''=0,v'}$ | FC | $E_{v''=0,v'}$ | FC | $E_{v''=0,v'}$ | FC | $E_{v''=0,v'}$ |
| 0 | 0.0010 | 6.169 | 0.0017 | 7.362 | 0.0611 | 7.353 | 0.0016 | 8.165 | 0.0019 | 8.398 | 0.0431 | 8.549 | 0.0031 | 8.895 | 0.5468 | 11.032 |
| 1 | 0.0052 | 6.347 | 0.0085 | 7.546 | 0.1477 | 7.569 | 0.0081 | 8.350 | 0.0094 | 8.585 | 0.1159 | 8.756 | 0.0141 | 9.085 | 0.3074 | 11.279 |
| 2 | 0.0148 | 6.521 | 0.0228 | 7.726 | 0.1954 | 7.772 | 0.0219 | 8.532 | 0.0250 | 8.769 | 0.1708 | 8.959 | 0.0349 | 9.273 | 0.1059 | 11.520 |
| 3 | 0.0301 | 6.692 | 0.0436 | 7.903 | 0.1907 | 7.976 | 0.0422 | 8.711 | 0.0472 | 8.950 | 0.1831 | 9.158 | 0.0618 | 9.457 | 0.0296 | 11.752 |
| 4 | 0.0487 | 6.859 | 0.0666 | 8.078 | 0.1512 | 8.177 | 0.0650 | 8.887 | 0.0711 | 9.128 | 0.1601 | 9.355 | 0.0877 | 9.639 | 0.0074 | 11.973 |
| 5 | 0.0672 | 7.023 | 0.0866 | 8.250 | 0.1054 | 8.374 | 0.0854 | 9.061 | 0.0916 | 9.303 | 0.1216 | 9.548 | 0.1062 | 9.818 | | |
| 6 | 0.0822 | 7.184 | 0.0999 | 8.419 | 0.0659 | 8.568 | 0.0989 | 9.231 | 0.1040 | 9.416 | 0.0832 | 9.737 | 0.1141 | 9.994 | | |
| 7 | 0.0915 | 7.340 | 0.1048 | 8.585 | 0.0388 | 8.757 | 0.1047 | 9.399 | 0.1080 | 9.645 | 0.0526 | 9.923 | 0.1118 | 10.166 | | |
| 8 | 0.0945 | 7.494 | 0.1019 | 8.748 | 0.0216 | 8.944 | 0.1031 | 9.563 | 0.1043 | 9.812 | 0.0313 | 10.106 | 0.1016 | 10.336 | | |
| 9 | 0.0919 | 7.644 | 0.0933 | 8.908 | 0.0114 | 9.126 | 0.0943 | 9.725 | 0.0934 | 9.976 | 0.0178 | 10.285 | 0.0870 | 10.504 | | |
| 10 | 0.0851 | 7.790 | 0.0813 | 9.065 | 0.0059 | 9.305 | 0.0827 | 9.884 | 0.0803 | 10.137 | 0.0098 | 10.461 | 0.0710 | 10.668 | | |
| 11 | 0.0757 | 7.932 | 0.0680 | 9.220 | 0.0029 | 9.480 | 0.0688 | 10.041 | 0.0655 | 10.295 | 0.0052 | 10.633 | 0.0557 | 10.830 | | |
| 12 | 0.0651 | 8.071 | 0.0549 | 9.372 | 0.0015 | 9.652 | 0.0560 | 10.194 | 0.0522 | 10.451 | 0.0027 | 10.803 | 0.0424 | 10.989 | | |
| 13 | 0.0545 | 8.205 | 0.0431 | 9.520 | 0.0007 | 9.819 | 0.0441 | 10.345 | 0.0405 | 10.604 | 0.0014 | 10.969 | 0.0314 | 11.146 | | |
| 14 | 0.0446 | 8.337 | 0.0331 | 9.666 | 0.0003 | 9.894 | 0.0356 | 10.492 | 0.0302 | 10.755 | 0.0007 | 11.131 | 0.0228 | 11.300 | | |
| 15 | 0.0357 | 8.464 | 0.0249 | 9.809 | 0.0002 | 10.144 | 0.0252 | 10.637 | 0.0223 | 10.902 | 0.0004 | 11.290 | 0.0163 | 11.452 | | |
| 16 | 0.0281 | 8.587 | 0.0184 | 9.949 | 0.0001 | 10.300 | 0.0188 | 10.780 | 0.0163 | 11.048 | | | 0.0115 | 11.601 | | |
| 17 | 0.0218 | 8.705 | 0.0134 | 10.086 | | | 0.0135 | 10.919 | 0.0115 | 11.190 | | | 0.0081 | 11.748 | | |
| 18 | 0.0167 | 8.820 | 0.0097 | 10.221 | | | 0.0097 | 11.056 | 0.0081 | 11.330 | | | 0.0056 | 11.891 | | |
| 19 | 0.0126 | 8.931 | 0.0069 | 10.350 | | | | | 0.0056 | 11.467 | | | | | | |
| 20 | 0.0093 | 9.037 | | | | | | | | | | | | | | |
| 21 | 0.0068 | 9.138 | | | | | | | | | | | | | | |

configuration $2s\sigma_u \rightarrow 2p\pi_g$ requires a spin-exchange electron collision to reach the final $C\,^3\Pi_u$ state. All dipole-allowed transitions (singlet states such as the $b\,^1\Pi_u$, $c\,^1\Pi_u$) lie above the present energy-loss region. Forbidden transitions are generally difficult to model because of the higher electric multipole interactions involved in the excitation of such transitions, as well as the complication of spin exchange if it is a singlet$\rightarrow$triplet transition. Further, given the considerable electron-electron correlation in the ground-state valence molecular orbitals, we can expect that any single-electron-type excitations would invoke a strongly coupled $N_2^+$ molecular core which can be expected to participate significantly in the overall scattering dynamics. Fortunately, in this region of energy loss (6.25–11.35 eV), the electronic states present all have different symmetries. This situation inhibits perturbative interactions (see Ref. [7], Sec. V.iii) which could complicate the derivation of FC factors—a situation that exists for higher-lying states of $N_2$. This means that reasonable FC factors can be obtained for this work and used to unfold the electron energy-loss spectrum in this region of energy loss.

The aim of the present experimental work is to investigate excitation of these eight lowest electronic states in $N_2$ over a wide impact-energy range, to fill the existing gap at low energy as well as to provide systematically reliable data at higher energies, using an improved experimental setup as well as improved data acquisition and analysis as compared to previous work. In the energy-loss spectra of $N_2$, the vibrational band structure for the eight lowest electronic states ($A\,^3\Sigma_u^+$, $B\,^3\Pi_g$, $W\,^3\Delta_u$, $B'\,^3\Sigma_u^-$, $a'\,^1\Sigma_u^-$, $a\,^1\Pi_g$, $w\,^1\Delta_u$, and $C\,^3\Pi_u$ from here on designated as $A,B,W,B',a',a,w,C$) heavily overlap and constitute a group of excitation features in the 6.2–11.4-eV electron energy-loss region. Even with the excellent experimental energy resolutions of 30–40 meV (full width at half maximum, FWHM) it is not possible to resolve any spectral features that appertain to single vibrational level(s) for any of the states other than the $A\,^3\Sigma_u^+ v'=0$ to $v'=6$ vibrational features. For practical reasons (which involve obtaining spectra with adequate statistics over reasonable time intervals), energy-loss spectra, obtained so far for the purpose of extracting excitation cross sections, were taken with resolutions of around 45 meV or greater. In such studies, experimentalists have relied on unfolding techniques which introduce additional uncertainty to the results because they rely heavily on our knowledge of the energy levels of the molecular states as well as the value of the FC factors which describe the intensity behavior of the individual vibrational excitations for the $v''=0$ ground-state vibrational level to the excited $v'=0,1,2\ldots$ levels, in the Born-Oppenheimer approximation (see, e.g., Ref. [9]) which allows one to uncouple the vibrational and electronic wave functions (during excitation) so that the vibrational wave functions are primarily dependent only on the internuclear coordinate $R$. Examples of such unfoldings are shown in Fig. 1. The unfolding errors propagate on top of the standard experimental

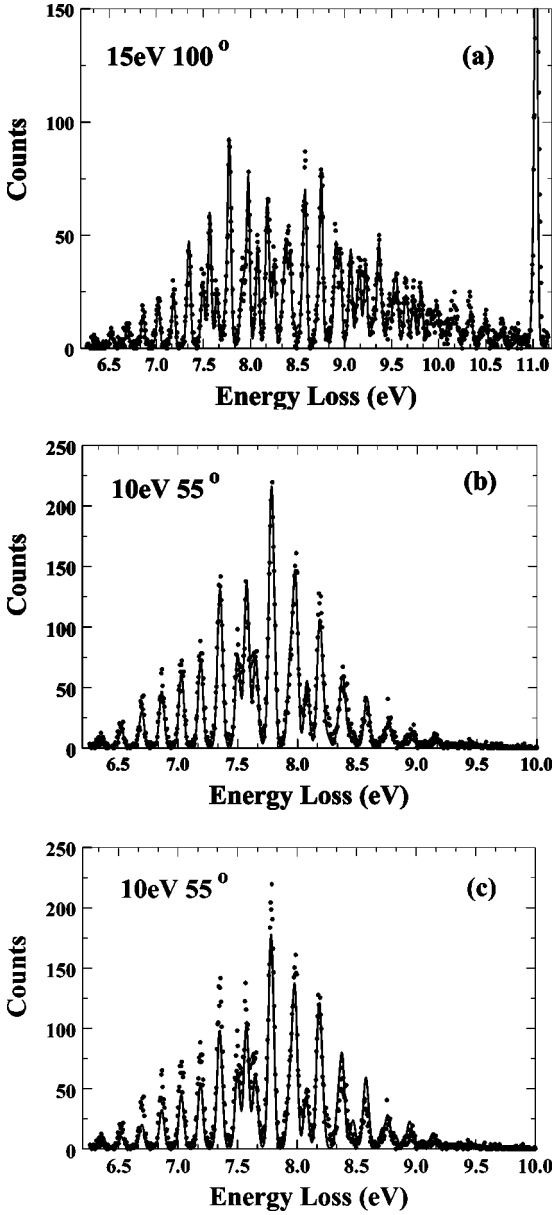


FIG. 1. (a) Energy-loss spectrum of $N_2$ taken at $\varepsilon_0=15$ V and $\theta=100°$. Dots are the experimental data and the line is the unfolding fit to the experimental data. The $\chi_\nu^2$ for the fit is 1.22. (b) Energy-loss spectrum of $N_2$ taken at $\varepsilon_0=10$ eV and $\theta=55°$. Same legend as (a), but fitted with flux-weighted FC factors. $\chi_\nu^2=1.45$. See text for details. (c) Same as (b) but fitted with unweighted FC factors. $\chi_\nu^2=4.22$. See text for details.

errors needed to determine the normalized (absolute) DCSs from the observed energy-loss spectra.

Work related to the excitation of these eight states can be briefly summarized as follows: Mazeau *et al.* [10] obtained relative differential excitation function curves for vibrational levels of the $A\ ^3\Sigma_u^+$ and $B\ ^3\Pi_g$ states from threshold to 12 and 13 eV, respectively, at several scattering angles. They also determined relative angular distribution curves at several impact energies for scattering angles up to 120°. Finn and Doering [11] reported relative differential and normalized integral cross sections for the $a\ ^1\Pi_g$ state in the 13–100-eV impact energy range with a moderate resolution of 120 meV. Their normalization was based on the $C\ ^3\Pi_u\ (v'=0)$ optical excitation function of Aarts and de Heer [12]. DCSs for the $A\ ^3\Sigma_u^+$, $B\ ^3\Pi_g$, $W\ ^3\Delta_u$, $B'\ ^3\Sigma_u^-$, $a'\ ^1\Sigma_u^-$, $a\ ^1\Pi_g$, $w\ ^1\Delta_u$, and $C\ ^3\Pi_u$ were measured by Cartwright *et al.* [13] at 10, 12.5, 15, 17, 20, 30, and 50 eV impact energies ($\varepsilon_0$) at scattering angles ($\theta$) ranging from 5 to 138° with an instrumental energy resolution of 40–60 meV. They also obtained integral cross sections from their data [14]. In their work, efforts were made to make the scattered electron detection efficiency independent of the residual energy by tuning the spectrometer so that the inelastic and elastic features were simultaneously maximized. However, no independent absolute calibration for the detector sensitivity was carried out. Furthermore, their background scattering correction was determined by drawing a smooth background curve in the energy-loss spectrum, relying on regions where no excitation features were present. Such procedures cannot account properly for the background contribution to the elastic scattering which suffers from secondary electrons produced from surfaces surrounding the collision region. Normalization of their cross sections was based on the DCSs for elastic scattering by $N_2$ by Srivastava *et al.* [15], that used existing elastic DCSs of He by McConkey and Preston [16] as a calibration standard via a relative flow method. Later, Trajmar *et al.* [1] corrected these cross sections on the basis of newer He DCSs taken by Register *et al.* [17]. Similar measurements at a higher resolution of 35–40 meV (FWHM) were carried out by Zetner and Trajmar [18] at the $\varepsilon_0$ value of 15 eV for $\theta$ up to 135°. They also used similar FC factors as those used by Cartwright *et al.* [13], but only considered the four strongest contributors to the energy-loss spectrum, viz. the *A*, *W*, *B*, and a state energy-loss features. Similar to Cartwright *et al.* [13] they attempted to make the scattered detector efficiency uniform by optimizing the inelastic and elastic signal. They also took proper account of their background, by shunting the target gas away from the collimating needle source and into a side leak [19]. Recently, Brunger and Teubner [3] measured DCSs for excitation of the above eight states plus the higher-lying $E\ ^3\Sigma_g^+$ and $a''\ ^1\Sigma_g^+$ states at $\varepsilon_0=15$, 17.5, 20, 30, and 50 eV in the 10–90° angular range also using FC factors similar to Cartwright *et al.* [13]. Their method was based on relatively normalized measurements to the $a''\ ^1\Sigma_g^+$ feature at 12.253 eV energy loss and subsequent absolute normalization to the elastic DCSs. The electron optics in their apparatus were designed and adjusted to be independent of electron residual energy. This was facilitated, up to 6 eV residual energy, using the near-threshold ionization energy loss spectrum of He (see, e.g., Ref. [19]). They measured their residual gas background by turning off their target beam completely, which would have left the secondary electron-scattering contribution due to electron-residual gas scattering from surfaces surrounding the collision region not completely accounted for. Allan [20] reported an investigation of energy-loss spectra at near threshold energies using a trochoidal electron gun and detector system. In the experiment the 0 and 180° combined differential scattering signal was detected and the energy dependence of the relative differential excitation functions for the $A\ ^3\Sigma_u^+(v'=6)$ and $B\ ^3\Pi_u$

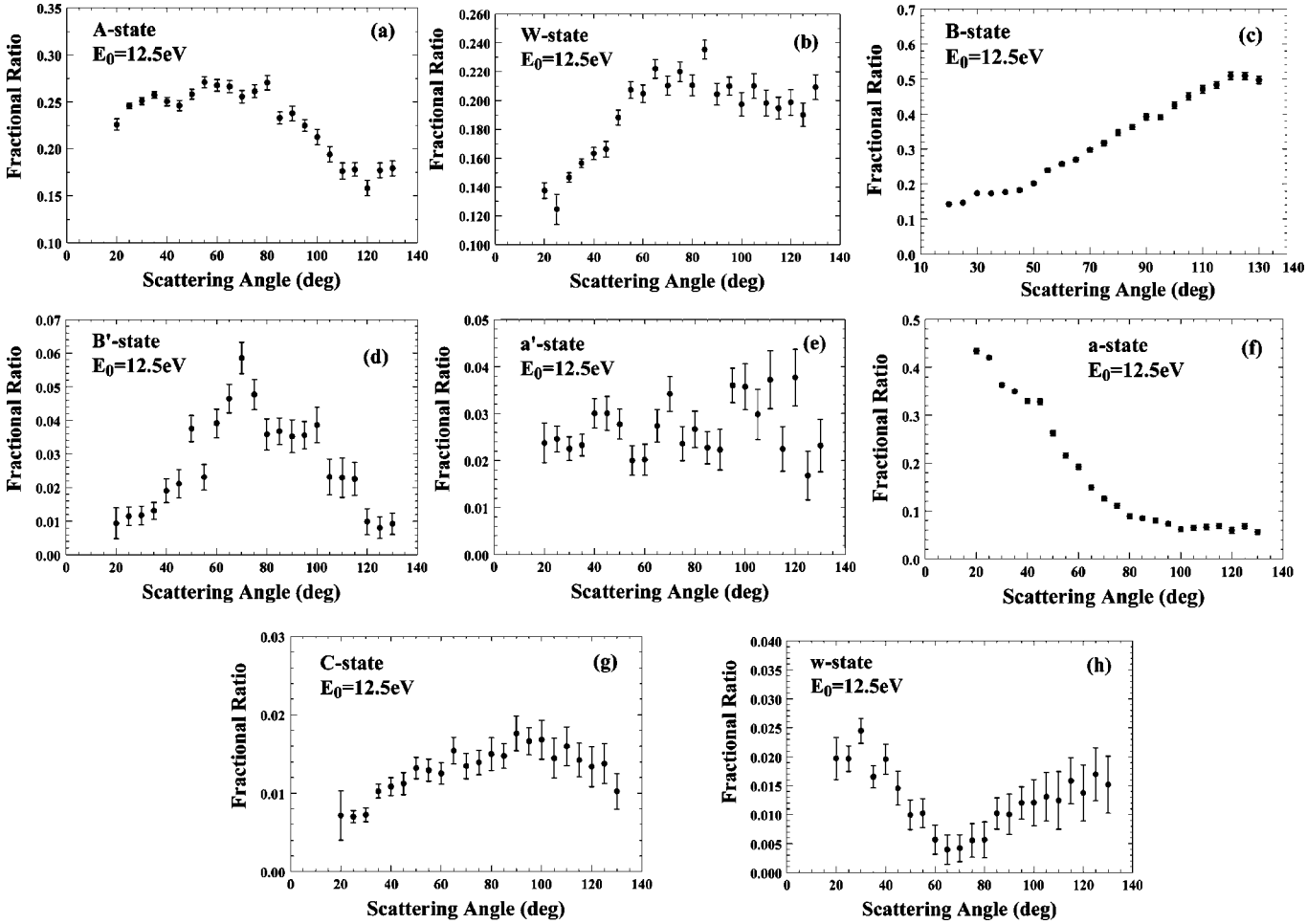


FIG. 2. The fractional ratio of *A*, *W*, *B*, *B′*, *a′*, *a*, *C*, and *w* states, respectively, to the $A+W+B+B'+a'+a+C+w$ spectrum at $\varepsilon_0 = 12.5$ eV, vs $\theta$. See text for details. Error bars include statistical and fitting (unfolding) uncertainties.

($v'=1$) excitations were given in the threshold to 12.0-eV range. Similar work using a double-trochoidal electron spectrometer by Poparić *et al.* [21] was reported on the $C\ ^3\Pi_u$ ($v'=0$, 1, and 2) levels from threshold to 17 eV and used to identify resonance contributions to these excitations. The (weak) $B'\ ^3\Sigma_u^-$ and $a'\ ^1\Sigma_u^-$ state excitation features are not present in the trochoidal spectrometer spectra as expected on the basis of symmetry arguments [22,23], for forward and backward scattering. Le Clair and Trajmar [24] measured accurate differential excitation cross sections for the sum of the seven lowest electronic states (Region I in their paper), a small fraction of the $w\ ^1\Delta_u$ and all the $C\ ^3\Pi_u$ state (Region II in their paper) at 90° in the 7.5 to 20-eV impact energy range using a uniform transmission time-of-flight (TOF) apparatus [25]. Combining these results with available medium resolution energy-loss spectra, they also deduced DCSs for excitation of the $A\ ^3\Sigma_u^+ v'=6$ and $v'=4,5,6$ excitations at 90° for 12, 15, and 20.7-eV impact energies. Ajello and Shemansky [26] (1985 and 1989) reported a re-examination of the $a\ ^1\Pi_g$ state integral excitation cross section based on optical measurements of the Lyman-Birge-Hopfield (LBH) bands. The relative optical excitation curve obtained by them was normalized at 100 eV to the Lyman-$\alpha$ production cross section from electron impact on $H_2$ by a relative-flow technique. Borst [27] derived integral cross sections in the threshold to 40-eV impact energy range for excitation of the *A* and *a* electronic states based on TOF measurements. Mason and Newell [28] measured relative cross sections for the production of $a\ ^1\Pi_g$ metastables by electron impact in the threshold to 150-eV impact-energy range. They normalized their results at 17 eV to the average of available integral cross sections of Cartwright *et al.* [13], Ajello and Shemansky [26], and Borst [27].

Significant progress has been made in the last few decades in the theoretical area concerning calculation of cross sections for electron molecule collision processes (see, e.g., Refs. [29,30]). However, these theoretical methods and approximations need to be checked against experimental data to assess their validity and to find the proper tradeoff between complexity and practicality. The most recent work regarding $N_2$ is that of Gillan *et al.* [31] who initially calculated DCSs for excitation of the $N_2$ *A*, *B*, and *W* states applying the *R*-matrix formalism. Following this, Gillan *et al.* [32] extended their *R*-matrix calculations for excitation of the $A\ ^3\Sigma_u^+$, $B\ ^3\Pi_g$, $W\ ^3\Delta_u$, $B'\ ^3\Sigma_u^-$, $a'\ ^1\Sigma_u^-$, $a\ ^1\Pi_g$, and $w\ ^1\Delta_u$ states of $N_2$ for incident energies from threshold up to 17 eV, obtaining improved agreement with the more recent experiments of Brunger and Teubner [3]. In their paper, Gillan *et al.* [32] graphically report DCSs for excitation of the $A\ ^3\Sigma_u^+$

TABLE III. Present inelastic (summed over the A+W+B+B′+a′+a+C+w states) to elastic electron scattering ratios for $N_2$ at the various $\varepsilon_0$ values. The ratios for $\varepsilon_0 < 30$ eV have been normalized to the ratios given by LeClair and Trajmar [24] at $\theta = 90°$. Only statistical errors are listed here. Additional errors (e.g., due to the elastic DCS) are added in evaluating the excitation DCSs. See text for discussion.

| $\theta$ (deg) | 10 eV | Error | 12.5 eV | Error | 15 eV | Error | 20 eV | Error | 30 eV | Error | 50 eV | Error | 100 eV | Error |
|---|---|---|---|---|---|---|---|---|---|---|---|---|---|---|
| 5 | | | | | | | | | 0.0226 | 0.0005 | 0.0202 | 0.0005 | | |
| 10 | | | | | 0.0174 | 0.0006 | 0.0185 | 0.0004 | 0.0220 | 0.0005 | 0.0200 | 0.0005 | 0.0194 | 0.0006 |
| 15 | | | | | 0.0209 | 0.0007 | 0.0235 | 0.0006 | 0.0231 | 0.0006 | 0.0208 | 0.0005 | | |
| 20 | | | 0.0088 | 0.0003 | 0.0253 | 0.0007 | 0.0269 | 0.0007 | 0.0249 | 0.0006 | 0.0220 | 0.0005 | 0.0205 | 0.0007 |
| 25 | 0.0140 | 0.0014 | 0.0111 | 0.0004 | 0.0287 | 0.0008 | 0.0294 | 0.0012 | 0.0262 | 0.0007 | 0.0224 | 0.0006 | | |
| 30 | 0.0170 | 0.0015 | 0.0147 | 0.0005 | 0.0341 | 0.0010 | 0.0335 | 0.0008 | 0.0281 | 0.0007 | 0.0227 | 0.0006 | 0.0227 | 0.0009 |
| 35 | 0.0192 | 0.0016 | 0.0183 | 0.0006 | 0.0364 | 0.0011 | 0.0376 | 0.0014 | 0.0290 | 0.0008 | 0.0232 | 0.0007 | | |
| 40 | 0.0215 | 0.0017 | 0.0215 | 0.0006 | 0.0406 | 0.0013 | 0.0369 | 0.0001 | 0.0321 | 0.0010 | 0.0268 | 0.0008 | 0.0278 | 0.0012 |
| 45 | 0.0260 | 0.0020 | 0.0253 | 0.0007 | 0.0501 | 0.0014 | 0.0415 | 0.0023 | 0.0316 | 0.0011 | 0.0309 | 0.0010 | | |
| 50 | 0.0298 | 0.0025 | 0.0320 | 0.0009 | 0.0592 | 0.0016 | 0.0450 | 0.0012 | 0.0371 | 0.0013 | 0.0403 | 0.0014 | 0.0356 | 0.0015 |
| 55 | 0.0330 | 0.0030 | 0.0387 | 0.0010 | 0.0694 | 0.0020 | 0.0565 | 0.0016 | 0.0442 | 0.0016 | 0.0505 | 0.0018 | | |
| 60 | 0.0402 | 0.0038 | 0.0469 | 0.0013 | 0.0894 | 0.0028 | 0.0693 | 0.0020 | 0.0613 | 0.0023 | 0.0642 | 0.0024 | 0.0376 | 0.0017 |
| 65 | 0.0477 | 0.0047 | 0.0614 | 0.0017 | 0.120 | 0.004 | 0.0981 | 0.0028 | 0.0845 | 0.0034 | 0.0850 | 0.0032 | | |
| 70 | 0.0604 | 0.0061 | 0.0795 | 0.0022 | 0.163 | 0.005 | 0.134 | 0.004 | 0.131 | 0.005 | 0.108 | 0.004 | 0.0377 | 0.0021 |
| 75 | 0.0707 | 0.0074 | 0.0964 | 0.0028 | 0.218 | 0.007 | 0.197 | 0.006 | 0.184 | 0.006 | 0.138 | 0.006 | | |
| 80 | 0.0860 | 0.0088 | 0.125 | 0.004 | 0.268 | 0.009 | 0.264 | 0.008 | 0.238 | 0.008 | 0.171 | 0.007 | 0.0346 | 0.0020 |
| 85 | 0.106 | 0.009 | 0.149 | 0.004 | 0.295 | 0.011 | 0.295 | 0.009 | 0.290 | 0.009 | 0.187 | 0.008 | | |
| 90 | 0.115 | 0.009 | 0.167 | 0.004 | 0.290 | 0.010 | 0.302 | 0.009 | 0.336 | 0.010 | 0.210 | 0.008 | 0.0323 | 0.0019 |
| 95 | 0.119 | 0.009 | 0.159 | 0.004 | 0.248 | 0.009 | 0.247 | 0.008 | 0.346 | 0.010 | 0.199 | 0.008 | | |
| 100 | 0.109 | 0.008 | 0.150 | 0.004 | 0.191 | 0.006 | 0.200 | 0.007 | 0.315 | 0.009 | 0.173 | 0.007 | 0.0298 | 0.0017 |
| 105 | 0.0964 | 0.0074 | 0.137 | 0.004 | 0.172 | 0.005 | 0.177 | 0.005 | 0.272 | 0.008 | 0.150 | 0.006 | | |
| 110 | 0.0878 | 0.0063 | 0.110 | 0.003 | 0.145 | 0.004 | 0.153 | 0.004 | 0.227 | 0.006 | 0.122 | 0.004 | 0.0285 | 0.0017 |
| 115 | 0.0719 | 0.0052 | 0.0873 | 0.0026 | 0.128 | 0.004 | 0.134 | 0.004 | 0.194 | 0.005 | 0.101 | 0.004 | | |
| 120 | 0.0643 | 0.0045 | 0.0751 | 0.0022 | 0.121 | 0.006 | 0.120 | 0.003 | 0.163 | 0.004 | 0.0858 | 0.0030 | 0.0266 | 0.0015 |
| 125 | 0.0574 | 0.0042 | 0.0657 | 0.0021 | 0.116 | 0.003 | 0.110 | 0.003 | 0.148 | 0.004 | 0.0714 | 0.0025 | | |
| 127 | 0.0543 | 0.0041 | | | | | | | | | | | | |
| 130 | | | 0.058 | 0.002 | 0.103 | 0.003 | 0.103 | 0.003 | 0.131 | 0.003 | 0.063 | 0.002 | 0.0228 | 0.0013 |

state at $\varepsilon_0 = 10$ and 15 eV, but concentrate on providing integral cross sections. However, to provide a more useful model for electron-$N_2$ scattering, differential results would provide a better picture.

## II. EXPERIMENTAL TECHNIQUES AND PROCEDURES

The experimental data reported here constitute the results of a collaboration between California State University, Fullerton (CSUF) and the Jet Propulsion Laboratory–California Institute of Technology (JPL-Caltech). Detailed descriptions of the CSUF apparatus are given in Khakoo *et al.* [33]. Cylindrical electrostatic optics and double hemispherical energy selectors were utilized both in the electron gun and the detector. Energy-loss spectra, including both the elastic peak and the inelastic region of interest, were collected at fixed impact energies and scattering angles by repetitive, multichannel-scaling techniques. The target $N_2$ beam was formed by effusing the gas through a capillary array (of 50 capillaries with a collimation ratio of 100, i.e., the ratio of the length of the array over the diameter of a single capillary) driven by a pressure of a few Torr behind it. The background signal was accurately determined using a moveable source method developed recently at CSUF [34]. This method has been demonstrated to be reliable both at JPL-Caltech and CSUF [35,36]. The incident energy $\varepsilon_0$ of the electron beam was determined by tuning the spectrometer analyzer to the elastic peak (energy loss: $E=0$) and then monitoring the energy-loss spectrum to the maximum cutoff in the energy-loss spectrum (at $E=\varepsilon_0$). The correct value of $\varepsilon_0$ could be set by adjusting the appropriate electron gun bias power supply to obtain the required cutoff voltage and this could be done to $<50$ meV. This provided an easier method than the usual method of using the $2\,^2S$ resonance in the electron-helium scattering elastic channel [33], and further gave excellent agreement with this method. The energy-loss cutoff method has the advantage, over the helium resonance method, that one does not have to change gases, but it is less precise.

The procedure for obtaining the normalized cross sections consisted of several steps:

(i) In the first step, the spectrometer was tuned such that the elastic to inelastic ratios reproduced closely those from the TOF work of LeClair and Trajmar [24] which are accu-

TABLE IV. Present DCSs and associated uncertainties at $\varepsilon_0=10$ eV, units: $\times 10^{-19}$ cm$^2$/sr.

| $\theta$ (deg) | $A\,^3\Sigma_u^+$ | Error | $W\,^3\Delta_u$ | Error | $B\,^3\Pi_g$ | Error | Sum | Error |
|---|---|---|---|---|---|---|---|---|
| 25 | 18.7 | 3.4 | 0.62 | 0.26 | 12.8 | 2.3 | 32.1 | 5.8 |
| 30 | 19.3 | 3.5 | 0.68 | 0.24 | 15.5 | 2.8 | 35.5 | 6.4 |
| 35 | 20.1 | 3.5 | 0.66 | 0.24 | 15.7 | 2.8 | 37.4 | 6.6 |
| 40 | 19.0 | 3.3 | 1.05 | 0.25 | 18.5 | 3.2 | 39.2 | 6.9 |
| 45 | 20.9 | 3.7 | 1.61 | 0.28 | 20.2 | 3.6 | 43.4 | 7.6 |
| 50 | 20.9 | 3.7 | 1.52 | 0.27 | 21.9 | 3.8 | 44.8 | 7.8 |
| 55 | 20.4 | 3.6 | 1.22 | 0.22 | 21.5 | 3.8 | 44.0 | 7.7 |
| 60 | 20.9 | 3.7 | 1.73 | 0.31 | 23.4 | 4.1 | 47.0 | 8.2 |
| 65 | 22.0 | 3.9 | 1.62 | 0.35 | 23.8 | 4.2 | 47.8 | 8.4 |
| 70 | 21.7 | 3.8 | 1.62 | 0.41 | 26.9 | 4.8 | 50.8 | 8.9 |
| 75 | 21.4 | 3.8 | 1.47 | 0.27 | 26.2 | 4.7 | 49.5 | 8.8 |
| 80 | 21.7 | 3.8 | 1.92 | 0.42 | 26.1 | 4.6 | 50.3 | 8.9 |
| 85 | 22.3 | 4.0 | 2.03 | 0.43 | 28.9 | 5.1 | 53.4 | 9.5 |
| 90 | 20.9 | 3.7 | 2.26 | 0.47 | 28.1 | 5.0 | 51.5 | 9.1 |
| 95 | 18.0 | 3.2 | 2.44 | 0.52 | 30.1 | 5.4 | 50.6 | 9.0 |
| 100 | 17.7 | 3.1 | 2.09 | 0.46 | 27.1 | 4.8 | 46.9 | 8.2 |
| 105 | 15.5 | 2.8 | 2.77 | 0.57 | 25.8 | 4.6 | 44.1 | 7.9 |
| 110 | 16.6 | 3.0 | 2.02 | 0.44 | 25.0 | 4.4 | 43.7 | 7.7 |
| 115 | 13.5 | 2.5 | 1.81 | 0.33 | 23.1 | 4.2 | 38.9 | 7.0 |
| 120 | 12.6 | 2.2 | 1.72 | 0.32 | 23.5 | 4.2 | 38.2 | 6.7 |
| 125 | 13.4 | 2.4 | 1.59 | 0.37 | 22.9 | 4.2 | 37.9 | 6.9 |
| 127 | 14.2 | 2.5 | 1.10 | 0.27 | 24.8 | 4.4 | 40.4 | 7.1 |

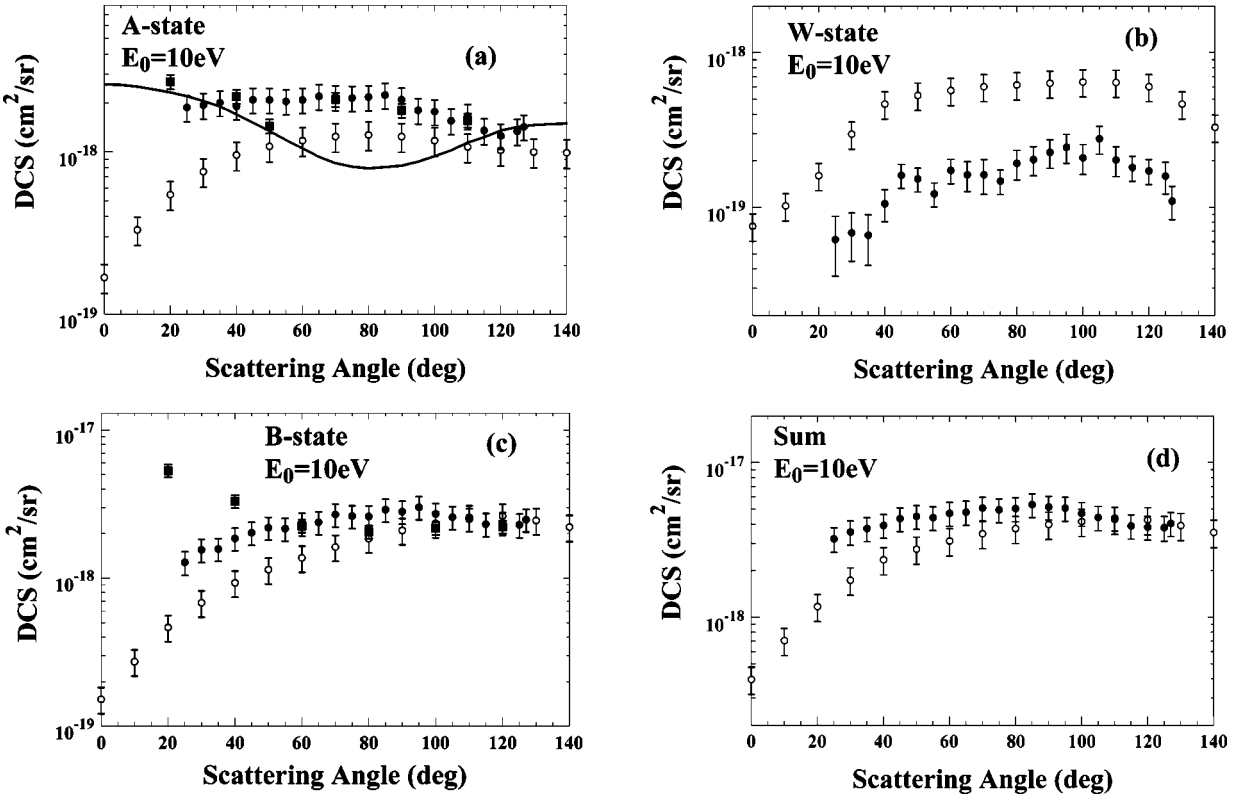


FIG. 3. DCSs for the electron impact excitation of the $A, W, B$ states of $N_2$ and their sum at $\varepsilon_0=10$ eV. Legend: ● Present work; ○ Ref. [13]; ■ Ref. [10];—*R* matrix, Ref. [32].

TABLE V. Present DCSs and associated uncertainties at $\varepsilon_0 = 12.5$ eV, units: $\times 10^{-19}$ cm$^2$/sr.

| $\theta$ (deg) | $A\,^3\Sigma_u^+$ | Error | $W\,^3\Delta_u$ | Error | $B\,^3\Pi_g$ | Error | $B'\,^3\Sigma_u^-$ | Error | $a'\,^1\Sigma_u^-$ | Error | $a\,^1\Pi_g$ | Error | $C\,^3\Pi_u$ | Error | $w\,^1\Delta_u$ | Error | Sum | Error |
|---|---|---|---|---|---|---|---|---|---|---|---|---|---|---|---|---|---|---|
| 20 | 6.03 | 0.98 | 3.67 | 0.61 | 3.80 | 0.62 | 0.25 | 0.13 | 0.63 | 0.15 | 11.6 | 1.9 | 0.19 | 0.09 | 0.53 | 0.13 | 26.7 | 4.3 |
| 25 | 7.38 | 1.44 | 3.74 | 0.73 | 4.41 | 0.86 | 0.34 | 0.07 | 0.74 | 0.14 | 12.6 | 2.2 | 0.21 | 0.04 | 0.59 | 0.12 | 30.0 | 4.8 |
| 30 | 8.77 | 1.40 | 5.13 | 0.83 | 6.07 | 0.97 | 0.41 | 0.12 | 0.79 | 0.15 | 12.7 | 2.0 | 0.25 | 0.05 | 0.86 | 0.16 | 35.0 | 5.6 |
| 35 | 9.76 | 1.56 | 5.94 | 0.95 | 6.58 | 1.05 | 0.50 | 0.12 | 0.88 | 0.17 | 13.3 | 2.1 | 0.39 | 0.07 | 0.63 | 0.12 | 37.9 | 6.0 |
| 40 | 9.68 | 1.55 | 6.31 | 1.02 | 6.84 | 1.09 | 0.74 | 0.18 | 1.16 | 0.22 | 12.8 | 2.0 | 0.42 | 0.08 | 0.76 | 0.16 | 38.7 | 6.1 |
| 45 | 9.72 | 1.56 | 6.57 | 1.06 | 7.22 | 1.16 | 0.83 | 0.21 | 1.19 | 0.24 | 13.0 | 2.1 | 0.44 | 0.09 | 0.58 | 0.15 | 39.5 | 6.3 |
| 50 | 11.1 | 1.8 | 8.13 | 1.31 | 8.73 | 1.40 | 1.62 | 0.31 | 1.20 | 0.23 | 11.3 | 1.8 | 0.57 | 0.11 | 0.43 | 0.13 | 43.2 | 6.8 |
| 55 | 12.0 | 1.9 | 9.16 | 1.47 | 10.6 | 1.7 | 1.02 | 0.23 | 0.88 | 0.20 | 9.53 | 1.53 | 0.57 | 0.11 | 0.45 | 0.13 | 44.2 | 7.0 |
| 60 | 11.9 | 1.9 | 9.11 | 1.47 | 11.5 | 1.8 | 1.74 | 0.34 | 0.90 | 0.20 | 8.56 | 1.38 | 0.56 | 0.11 | 0.25 | 0.12 | 44.5 | 7.1 |
| 65 | 12.9 | 2.1 | 10.7 | 1.7 | 13.0 | 2.1 | 2.25 | 0.41 | 1.32 | 0.27 | 7.21 | 1.17 | 0.75 | 0.14 | 0.19 | 0.13 | 48.4 | 7.7 |
| 70 | 13.2 | 2.1 | 10.9 | 1.8 | 15.4 | 2.5 | 3.03 | 0.54 | 1.77 | 0.34 | 6.50 | 1.06 | 0.70 | 0.14 | 0.22 | 0.13 | 51.7 | 8.2 |
| 75 | 13.4 | 2.2 | 11.3 | 1.8 | 16.3 | 2.6 | 2.45 | 0.45 | 1.21 | 0.27 | 5.69 | 0.94 | 0.71 | 0.14 | 0.29 | 0.16 | 51.3 | 8.1 |
| 80 | 14.9 | 2.4 | 11.6 | 1.9 | 19.1 | 3.1 | 1.97 | 0.40 | 1.47 | 0.32 | 4.90 | 0.82 | 0.83 | 0.17 | 0.31 | 0.18 | 55.1 | 8.7 |
| 85 | 13.5 | 2.2 | 13.7 | 2.2 | 21.0 | 3.4 | 2.14 | 0.41 | 1.32 | 0.29 | 4.93 | 0.82 | 0.86 | 0.16 | 0.59 | 0.18 | 58.1 | 9.2 |
| 90 | 14.7 | 2.4 | 12.6 | 2.1 | 24.3 | 3.9 | 2.18 | 0.46 | 1.38 | 0.35 | 4.94 | 0.84 | 1.09 | 0.22 | 0.62 | 0.24 | 61.8 | 9.8 |
| 95 | 13.5 | 2.2 | 12.6 | 2.0 | 23.6 | 3.8 | 2.14 | 0.42 | 2.17 | 0.41 | 4.39 | 0.74 | 1.00 | 0.19 | 0.72 | 0.20 | 60.2 | 9.5 |
| 100 | 12.9 | 2.1 | 12.0 | 2.0 | 25.8 | 4.1 | 2.35 | 0.49 | 2.17 | 0.45 | 3.74 | 0.67 | 1.02 | 0.22 | 0.73 | 0.27 | 60.8 | 9.6 |
| 105 | 11.7 | 1.9 | 12.7 | 2.1 | 27.1 | 4.4 | 1.40 | 0.39 | 1.80 | 0.43 | 3.92 | 0.71 | 0.87 | 0.21 | 0.79 | 0.28 | 60.2 | 9.6 |
| 110 | 9.31 | 1.55 | 10.5 | 1.7 | 24.8 | 4.0 | 1.21 | 0.37 | 1.96 | 0.45 | 3.50 | 0.64 | 0.84 | 0.19 | 0.66 | 0.28 | 52.8 | 8.4 |
| 115 | 8.27 | 1.36 | 9.04 | 1.48 | 22.4 | 3.6 | 1.05 | 0.28 | 1.04 | 0.28 | 3.19 | 0.56 | 0.66 | 0.15 | 0.74 | 0.22 | 46.4 | 7.4 |
| 120 | 7.01 | 1.17 | 8.81 | 1.45 | 22.6 | 3.6 | 0.437 | 0.19 | 1.67 | 0.38 | 2.63 | 0.49 | 0.59 | 0.15 | 0.61 | 0.24 | 44.3 | 7.0 |
| 125 | 7.60 | 1.26 | 8.15 | 1.34 | 21.8 | 3.5 | 0.344 | 0.15 | 0.72 | 0.25 | 2.94 | 0.52 | 0.59 | 0.14 | 0.73 | 0.23 | 42.9 | 6.8 |
| 130 | 7.67 | 1.27 | 8.95 | 1.47 | 21.3 | 3.4 | 0.396 | 0.15 | 0.99 | 0.29 | 2.41 | 0.44 | 0.44 | 0.12 | 0.65 | 0.23 | 42.8 | 6.8 |

rate on a relative scale to ±5%. The result was that over a range of $\varepsilon_0$ from 10 to 20 eV, the elastic to inelastic ratios followed (relatively) the DCSs of the TOF data to within ≈8%. This served to make the analyzer response roughly (within ≈8%) constant as required for unfolding the energy-loss spectra. The analyzer was baked and maintained in a very clean vacuum environment so that this response remained stable. At low residual energy $E_R$ $(=\varepsilon_0 - E)$ the transmission could be closely (within 10%) described by the function

$$T(E_R) = 0.0458 \ln(E_R) + 0.8189. \quad (1)$$

This function was applied to the spectrum obtained at $\varepsilon_0 = 10$ and 12.5 eV only, since these were the spectra affected outside of error bars at $E_R < 4$ eV. When this correction was made at $\varepsilon_0 \geqslant 15.0$ eV, it was found not to affect the unfolding significantly, i.e., by less than 5%.

(ii) We now accumulated energy-loss spectra in the energy-loss range of 6.25–11.25 eV, and unfolded these to obtain relative intensities of the *A*, *W*, *B*, *B'*, *a'*, *c*, *w*, and *C'* states using FC factors from a combination of data from Cartwright *et al.* [13], Benesch *et al.* [37], and Tanaka *et al.* [38]. The unfolding procedure has been described in detail by Wrkich *et al.* [6]. In this case, the molecular spectrum in terms of intensity $S_i(\varepsilon_0, \theta, E)$ vs energy loss ($E_i$ corresponding to the "*i*th" multichannel bin $(i = 1, 2, \ldots, I)$ of the spectrum with $E_i = E_1 + (i-1)\delta$E. Here, $\delta$E is the energy-loss step size per bin. The energy-loss spectrum taken at the fixed incident energy $\varepsilon_0$ and scattering angle $\theta$ was fitted to the function [6].

$$S_i(\varepsilon_0, \theta, E_i) = C \sum_{n'} \sigma_{n'}(\varepsilon_0, \theta) \sum_{v'} q_{n',v'} F(E_i - E_{n',v'}) + B(\varepsilon_0, \theta, E_i, \rho, I_0), \quad (2)$$

except that in this case the normalized instrumental line function,

$$F(E - E_{n',v'}) = \sum_{m=1}^{M} \frac{A_m}{\Delta_m \sqrt{\pi}} \exp\left[ -\left( \frac{E - E_{n',v'} - E_m}{\Delta_m} \right)^2 \right], \quad (3)$$

is a multi-Gaussian function (with *M* possible up to 5 and, with each Gaussian located off the line center by the energy-loss amount $E_m$, relative intensity $A_m$, and having the width $\Delta_m$. Note: In this work, we used *M* values that were ⩽2). Here, $E_{n',v'}$ is the energy-loss value for the $v'$ vibrational level for the $n'$ electronic state (see Table II). The function *F* in Eq. (3), was synthesized from a nonlinear least-squares fitting to an isolated feature (e.g., the $A\,^3\Sigma_u^+$ ($v' = 5$ or 6) feature) in the energy-loss spectrum or the $a\,^1\Pi_g$ ($v' = 0,1,2$) feature at small $\theta$ when this state dominated the energy-loss spectrum. In Eq. (2), the $q_{n',v'}$ are the FC factors for the vibrational transitions $X\,^1\Sigma_g^+(v''=0) \rightarrow n'(v')$ in the elec-

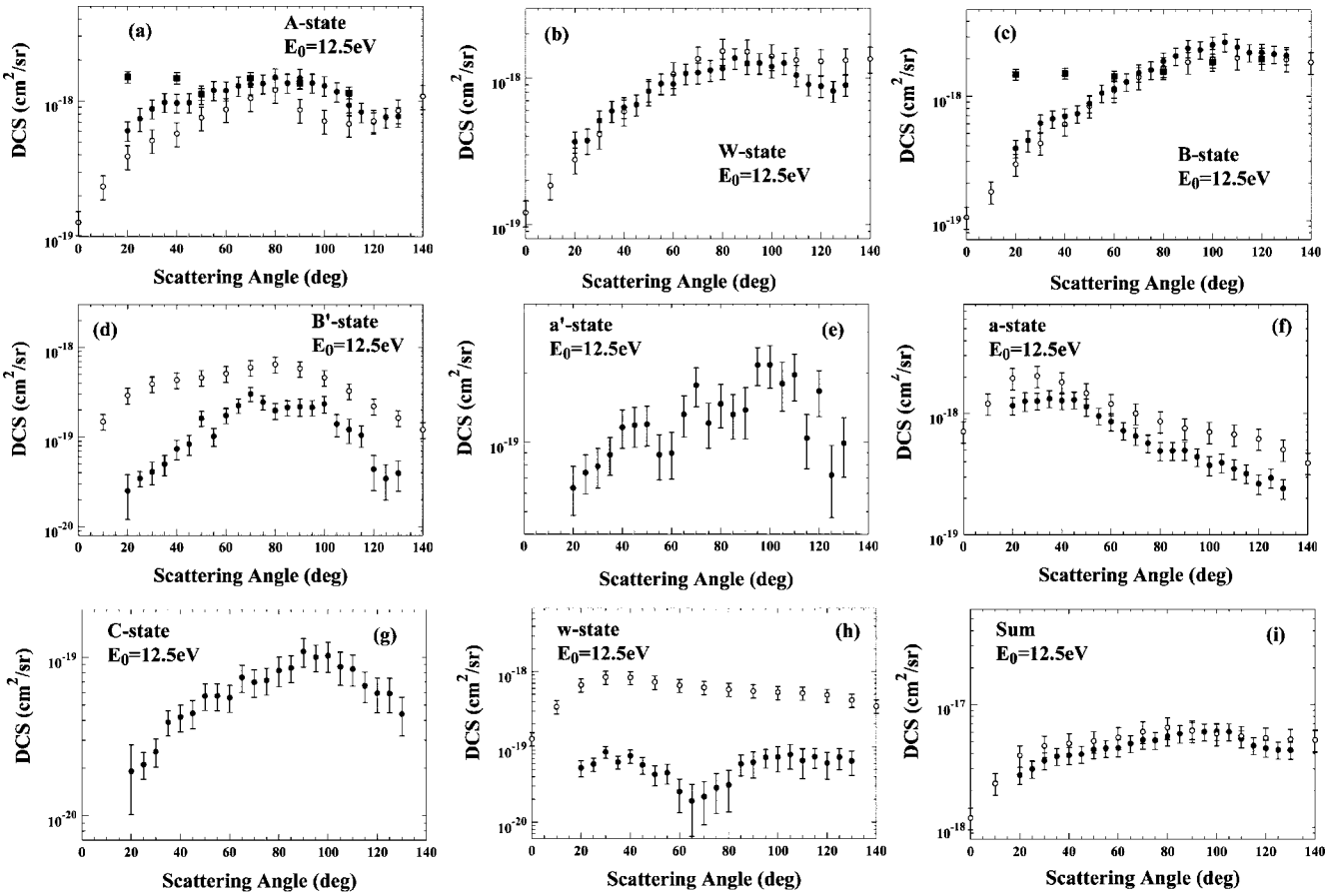


FIG. 4. DCSs for the electron impact excitation of the *A*, *W*, *B*, *B′*, *a′*, *a*, *C*, and *w* states of $N_2$ and their sum at $\varepsilon_0=12.5$ eV. Legend is the same as Fig. 3 except that Ref. [10] data are at $\varepsilon_0=12$ eV for the *A* state and $\varepsilon_0=13$ eV for the *B* state. Note that Ref. [13] DCSs are scaled down by 0.63. See text for discussion.

tronic manifold $n'$. These FC factors are given in Table II and arranged according to the electronic state's $n$ value [see Eq. (2)], where $n$ ranges from 1 to 8. Transition energies and FC factors for the $X(v''=0) \rightarrow A, W, B, B', a', a(v')$ transitions were taken from the compilation of Cartwright et al. [13] and were all found to agree excellently with those provided by Gilmore et al. [39], in most cases to better than 2%. We note that these FC factors were those used in the work of Zetner and Trajmar [18]. At this point we stress the need to present (in tabular form) FC factors used, when reporting unfolded molecular data. This point will also be elaborated on later in the discussion of our results. The $\sigma_{n'}(\varepsilon_0,\theta)$ are the DCSs for the excitation of the electronic state $n'$. $C$ is the normalization constant. The function

$$B(\varepsilon_0,\theta,E,\rho,I_0), = \sum_{k=0}^{k<3} B_k E^k \qquad (4)$$

which represented the background was expressed as a polynomial of up to order 2 and was dependent on the incident electron current $I_0$ and target gas density distribution $\rho$. In Eqs. (2) and (4), the variables $C\sigma_{n'}(\varepsilon_0,\theta)$ and $B_i$ were determined by linear least-squares fitting to the spectrum [note: the $\sigma_{n'}(\varepsilon_0,\theta)$ will later be determined from the relative $C\sigma_{n'}(\varepsilon_0,\theta)$ values upon normalization to a known cross section). Two further features to improve the fits to the spectrum were the following:

(a) The function in Eq. (2) could be varied nonlinearly in $E$, to further minimize the residual of the fit, i.e., energy loss at the start of the spectrum $E_1$ was changed in successively reduced increments until a minimum in the reduced chi-squared value ($\chi_\nu^2$) was reached. Importantly, it was observed that the resultant minimum in $\chi_\nu^2$ was (uniquely) global for the spectrum.

(b) The step size $\delta E$ (=energy loss per unit bin) was varied in very small amounts, in collaboration with (a), to minimize $\chi_\nu^2$. The linearity in the computer ramp voltage (provided by a 0–10 V 12-bit digital-analog converter) to the power supplies that control the analyzer (detector) side of the spectrometer and therefore determine the energy-loss value, was typically ±2 mV in a 5 V span. However, the improvements in $\chi_\nu^2$ that were observed when doing this secondary correction were significantly smaller than in (a), and typically a factor of less than 0.1 of the changes in (a). This is because $\delta E$ did not vary significantly during the course of the experiment.

Steps (a) and (b) resulted in improved fits as gauged from $\chi_\nu^2$ values which were typically in the range of 1–3 for typically 1000 data points with $<13$ variables (i.e., the number of degrees of freedom, $\nu \approx 987$). A typical unfolded spectrum

TABLE VI. Present DCSs and associated uncertainties at $\varepsilon_0=15$ eV, units: $\times 10^{-19}$ cm$^2$/sr.

| $\theta$ (deg) | $A\,^3\Sigma_u^+$ | Error | $W\,^3\Delta_u$ | Error | $B\,^3\Pi_g$ | Error | $B'\,^3\Sigma_u^-$ | Error | $a'\,^1\Sigma_u^-$ | Error | $a\,^1\Pi_g$ | Error | $C\,^3\Pi_u$ | Error | $w\,^1\Delta_u$ | Error | Sum | Error |
|---|---|---|---|---|---|---|---|---|---|---|---|---|---|---|---|---|---|---|
| 10 | 11.7 | 2.1 | 7.30 | 1.34 | 3.58 | 0.67 | 0.26 | 0.34 | 0.56 | 0.34 | 50.1 | 8.9 | 3.58 | 0.66 | 4.84 | 0.91 | 82.0 | 14.5 |
| 15 | 10.9 | 1.9 | 6.39 | 1.18 | 3.74 | 0.69 | 0.22 | 0.34 | 0.54 | 0.38 | 53.8 | 9.4 | 4.29 | 0.78 | 5.47 | 1.03 | 85.4 | 14.9 |
| 20 | 10.8 | 1.9 | 6.30 | 1.19 | 3.83 | 0.72 | 0.24 | 0.44 | 0.47 | 0.43 | 54.3 | 9.5 | 7.57 | 1.37 | 5.67 | 1.07 | 89.2 | 15.6 |
| 25 | 9.43 | 1.67 | 6.36 | 1.15 | 4.23 | 0.76 | 0.35 | 0.32 | 0.49 | 0.33 | 51.0 | 8.9 | 8.91 | 1.57 | 6.08 | 1.10 | 86.9 | 15.2 |
| 30 | 8.16 | 1.44 | 7.62 | 1.36 | 5.33 | 0.95 | 1.80 | 0.41 | 1.47 | 0.37 | 48.7 | 8.5 | 9.43 | 1.66 | 5.34 | 0.96 | 87.8 | 15.3 |
| 35 | 8.12 | 1.43 | 7.97 | 1.42 | 5.57 | 0.99 | 3.20 | 0.61 | 1.91 | 0.41 | 38.6 | 6.7 | 9.45 | 1.66 | 4.09 | 0.74 | 78.9 | 13.8 |
| 40 | 7.38 | 1.30 | 8.40 | 1.49 | 6.58 | 1.16 | 4.77 | 0.87 | 3.71 | 0.69 | 29.5 | 5.2 | 9.86 | 1.74 | 3.35 | 0.62 | 73.6 | 12.9 |
| 45 | 7.97 | 1.41 | 8.50 | 1.51 | 8.01 | 1.41 | 5.80 | 1.04 | 4.25 | 0.78 | 26.1 | 4.6 | 11.1 | 2.0 | 3.35 | 0.62 | 75.1 | 13.1 |
| 50 | 9.14 | 1.61 | 9.86 | 1.74 | 7.98 | 1.40 | 5.73 | 1.03 | 4.00 | 0.73 | 20.5 | 3.6 | 12.2 | 2.1 | 3.30 | 0.61 | 72.7 | 12.7 |
| 55 | 9.85 | 1.74 | 9.38 | 1.66 | 8.83 | 1.56 | 6.40 | 1.15 | 3.75 | 0.70 | 15.3 | 2.7 | 12.4 | 2.2 | 3.23 | 0.61 | 69.2 | 12.1 |
| 60 | 10.9 | 1.9 | 11.7 | 2.1 | 9.46 | 1.69 | 5.40 | 1.02 | 3.81 | 0.76 | 13.4 | 2.4 | 14.2 | 2.5 | 2.84 | 0.59 | 71.8 | 12.5 |
| 65 | 14.1 | 2.5 | 12.4 | 2.2 | 11.9 | 2.1 | 5.72 | 1.04 | 4.07 | 0.76 | 11.4 | 2.0 | 13.9 | 2.5 | 3.91 | 0.72 | 77.4 | 13.5 |
| 70 | 13.2 | 2.3 | 14.0 | 2.5 | 13.1 | 2.3 | 6.66 | 1.21 | 4.41 | 0.82 | 9.18 | 1.64 | 17.6 | 3.1 | 5.51 | 1.01 | 83.7 | 14.7 |
| 75 | 18.3 | 3.2 | 17.0 | 3.0 | 15.2 | 2.7 | 4.87 | 0.90 | 3.73 | 0.71 | 9.43 | 1.68 | 17.6 | 3.1 | 4.76 | 0.87 | 90.9 | 15.9 |
| 80 | 17.8 | 3.1 | 17.8 | 3.1 | 15.2 | 2.7 | 5.06 | 0.94 | 3.34 | 0.65 | 8.35 | 1.49 | 19.7 | 3.5 | 5.38 | 0.98 | 92.7 | 16.2 |
| 85 | 15.6 | 2.7 | 17.2 | 3.0 | 15.1 | 2.7 | 4.56 | 0.83 | 3.74 | 0.69 | 7.74 | 1.37 | 19.9 | 3.5 | 5.08 | 0.91 | 88.9 | 15.6 |
| 90 | 13.6 | 2.4 | 17.1 | 3.1 | 15.1 | 2.7 | 4.31 | 0.86 | 3.02 | 0.64 | 7.35 | 1.35 | 16.8 | 3.0 | 3.78 | 0.74 | 81.1 | 14.2 |
| 95 | 10.9 | 1.9 | 14.8 | 2.6 | 13.5 | 2.4 | 3.57 | 0.67 | 2.82 | 0.54 | 5.99 | 1.07 | 13.8 | 2.4 | 3.64 | 0.67 | 69.0 | 12.1 |
| 100 | 8.70 | 1.54 | 12.3 | 2.2 | 11.1 | 2.0 | 2.83 | 0.53 | 2.41 | 0.46 | 5.08 | 0.91 | 11.2 | 2.0 | 3.02 | 0.56 | 56.6 | 9.9 |
| 105 | 7.21 | 1.29 | 12.7 | 2.3 | 12.4 | 2.2 | 3.31 | 0.63 | 2.27 | 0.45 | 4.94 | 0.90 | 11.6 | 2.1 | 2.54 | 0.49 | 57.0 | 10.0 |
| 110 | 6.90 | 1.22 | 13.6 | 2.4 | 12.5 | 2.2 | 3.17 | 0.59 | 2.01 | 0.39 | 5.06 | 0.90 | 9.6 | 1.7 | 2.26 | 0.42 | 55.1 | 9.6 |
| 115 | 6.24 | 1.10 | 13.6 | 2.4 | 12.1 | 2.1 | 3.45 | 0.63 | 2.28 | 0.43 | 5.26 | 0.93 | 10.8 | 1.9 | 2.92 | 0.53 | 56.7 | 9.9 |
| 120 | 6.89 | 1.23 | 15.5 | 2.7 | 13.9 | 2.4 | 3.61 | 0.68 | 2.40 | 0.47 | 5.26 | 0.95 | 11.6 | 2.1 | 2.75 | 0.52 | 61.9 | 10.8 |
| 125 | 7.90 | 1.46 | 17.7 | 3.2 | 15.8 | 2.9 | 3.57 | 0.73 | 2.68 | 0.58 | 5.25 | 1.00 | 13.9 | 2.5 | 1.85 | 0.43 | 68.7 | 12.2 |
| 130 | 8.84 | 1.56 | 18.3 | 3.2 | 15.4 | 2.7 | 3.62 | 0.67 | 2.23 | 0.44 | 5.06 | 0.91 | 13.7 | 2.4 | 2.67 | 0.50 | 69.8 | 12.2 |

is shown in Fig. 1(a). The spectrometer was found to be very stable, yielding currents of about 7–10 nA with an energy resolution of 33–40 meV (FWHM). To keep track of the reliability of our unfolding method, each spectrum was unfolded after acquisition and from it the fractional intensity of each individual state over the full $A+W+B+B'+a'+a+w+C$ intensity was monitored as a function of $\theta$ at the fixed $\varepsilon_0$ value. This process took place during the course of the experimental data acquisition. This simple step was critical in monitoring the experimental stability, checking for reproducibility, and whether statistics were adequate for unfolding. Spectra were retaken to check for reproducibility, usually not more than twice. A typical average sample of these ratios is shown, e.g., for $\varepsilon_0=12.5$ eV in Fig. 2. These fractions gave a good indication of the robustness of the unfolding method and, as just mentioned, the additional time required to achieve adequate statistics so that the errors on the unfolded individual electronic excitations were reasonable. Keeping track of the trend in these fractions was a useful tool in monitoring the merit of our unfolding method.

(iii) At this point the method described by Nickel *et al.* [19] using the elastic electron-$N_2$ DCSs was carried out to place our total $A+W+B+B'+a'+a+w+C$ intensities on an absolute DCS scale as follows:

(a) First using the moveable source method [34] we simultaneously measured the elastic spectrum (−0.25–+0.25 eV energy loss) and inelastic energy-loss spectrum (6–11.5 eV energy loss) with the gas source aligned into the electron beam (signal+background; IN) and then moved out of alignment (background; OUT). The subtracted result of the OUT spectrum from the IN spectrum could be used to determine the relative DCS of the summed $A+W+B+B'+a'+a+w+C$ states. Note that the spectrum was determined with lower statistics than that of the spectra in (ii), i.e., a lower number of channels were used and also fewer scans, since we did not need to unfold such spectra. However, the summed statistical uncertainty was always better than 3% on average after subtraction of the background.

(b) Relative DCSs were then obtained by normalizing the elastic peak counts to an average of selected experimental DCSs for elastic electron scattering from $N_2$ of Shyn and Carignan [40], Srivastava *et al.* [15] (renormalized by Trajmar *et al.* [1]), Nickel *et al.* [41], and Gote and Ehrhardt [42]. These data are tabulated in Trajmar *et al.* [1] and Brunger and Buckman [3]. In our selection, we used those values of elastic scattering DCSs for which the measurements showed agreement with each other within error bars.

(c) We renormalized the summed DCS data, obtained in (iii a), using the inelastic to elastic DCS ratios obtained from the TOF measurements of LeClair and Trajmar [24] at $\theta=90°$, which should be very reliable and have an absolute uncertainty of 16%. These normalized inelastic to elastic ra-

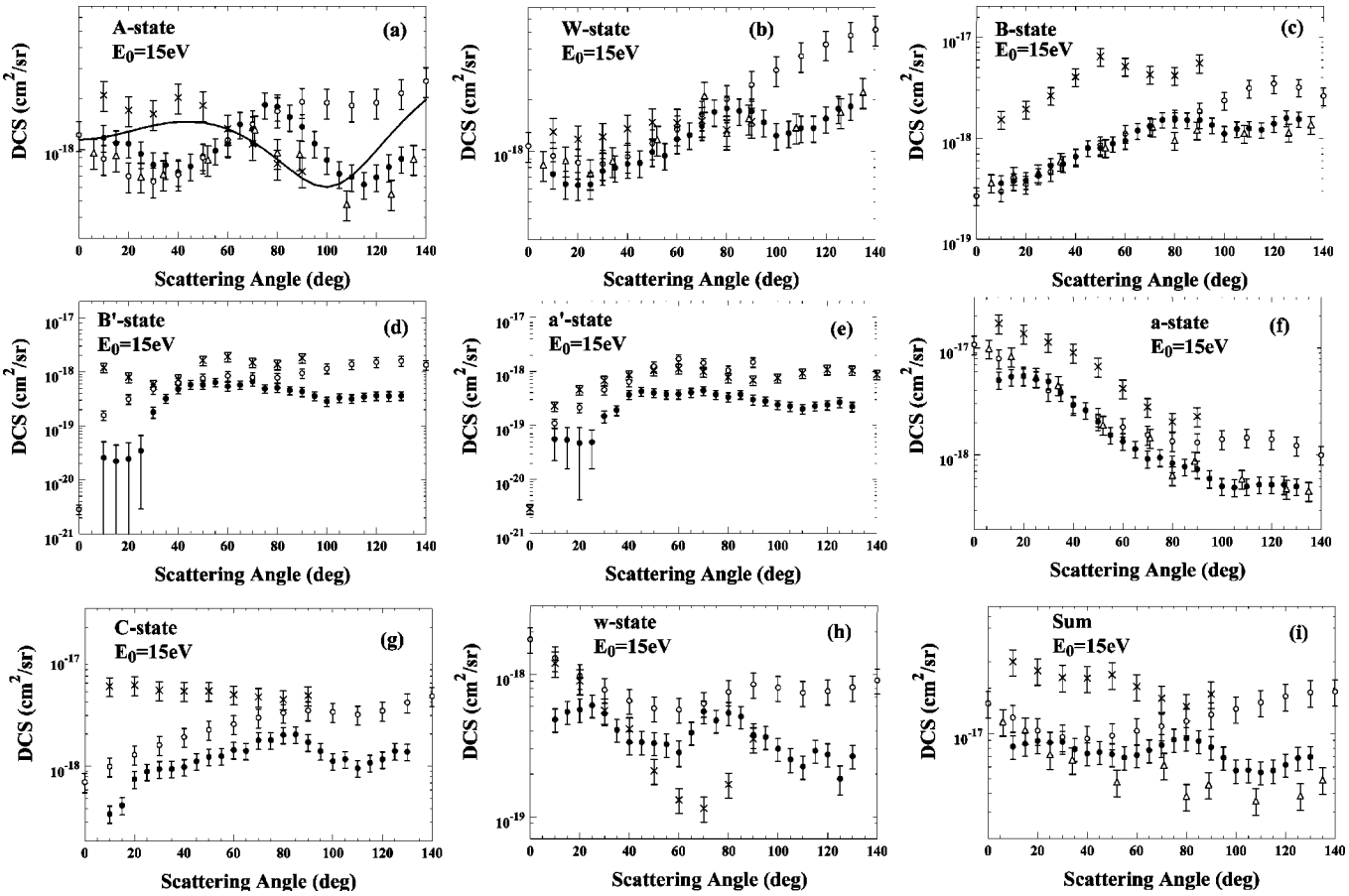


FIG. 5. DCSs for the electron impact excitation of the *A*, *W*, *B*, *B′*, *a′*, *a*, *C*, and *w* states of $N_2$ and their sum at $\varepsilon_0=15$ eV. Legend is the same as Fig. 3, but: ×, Ref. [3] and △, Ref. [18] scaled by the factor 0.45 (see text).

tios are listed in Table III. From this, applying the earlier individual state fractional intensities obtained in (ii), the individual state DCSs were finally obtained. In these procedures, we observed that compared to the LeClair and Trajmar [24] data at $\varepsilon_0 \geqslant 12.5$ eV, the correction to our analyzer response (elastic to inelastic ratio) was small, i.e., less than 12%. This correction factor serves to affirm the stability of the spectrometer and the fact that it maintained a uniform transmission over the spectrum as set up in Sec. II (i) for different $E_R$ electrons. At $\varepsilon_0=10$ eV this analyzer response correction was about 27%. At $\varepsilon_0 \leqslant 15$ eV, the method of flux-weighted FC factors, obtained by substituting $q_{n'v'}$ with $q^F_{n'v'}$ given by

$$q^F_{n',v'} = N_{n'} \frac{k_i}{k_f} q_{n',v'}, \tag{5}$$

where $k_i(\propto\sqrt{\varepsilon_0})$ and $k_f(\propto\sqrt{E_R})$ are the incident and scattered electron momenta [19,3], was applied and was found to work excellently, with great improvement to the fitting of the spectrum ($\chi^2_\nu$ values dropping from $>5$ on average to between 2.5 and 1). In Eq. (5), $N_{n'}$ is a normalization factor which ensures the sum of the flux-weighted FC factors for the electronic state (in this case the $n'$th state) equals 1. A typical spectrum taken at $\varepsilon_0=10$ eV and fitted using flux-weighted FC factors is shown in Fig. 1(b) and this is compared to the same spectrum fitted with regular (unweighted) FC factors [Fig. 1(c)], to show this improvement. At $\varepsilon_0>15$ eV, we found little difference in applying flux-weighted FC factors to the fit as compared to the normal (unweighted) FC factors. We also applied the following function $G(E_R)$ to correct the FC factors at low energy of the form:

$$G(E_R) = 1 - \exp - \left[\frac{E_R}{\alpha}\right]^2 \tag{6}$$

instead of $k_i/k_f$, in Eq. (5), but which has the asymptotic value of 1 when $E_i \to \infty$. In this case, the best value of $\alpha$ (=2.5) was found from applying trial $\alpha$ values in Eq. (6) to obtain a best fit to the spectra, i.e., a minimum in the $\chi^2_\nu$. Noticeable differences in the two methods in the region of ≈15% were observed at $\varepsilon_0=10$ eV, ≈8% at $\varepsilon_0=12.5$ eV, and >5% at $\varepsilon_0=15$ eV. These (estimated) uncertainties are also incorporated into our data because of the systematic uncertainty in applying a correction at near-threshold to the energy-loss spectra.

The experimental error, assigned to the various quantities, is the square root of the sum of the squares of the contributing error components. Here all errors are quoted to one standard deviation. For the DCS values associated with the sum of the eight state excitations at 90°, we considered the statis-

TABLE VII. Present DCSs and associated uncertainties at $\varepsilon_0 = 17.5$ eV, units: $\times 10^{-19}$ cm$^2$/sr.

| $\theta$ (deg) | $A\,^3\Sigma_u^+$ | Error | $W\,^3\Delta_u$ | Error | $B\,^3\Pi_g$ | Error | $B'\,^3\Sigma_u^-$ | Error | $a'\,^1\Sigma_u^-$ | Error | $a\,^1\Pi_g$ | Error | $C\,^3\Pi_u$ | Error | $w\,^1\Delta_u$ | Error | Sum | Error |
|---|---|---|---|---|---|---|---|---|---|---|---|---|---|---|---|---|---|---|
| 10 | 2.49 | 0.44 | 2.94 | 0.94 | 1.93 | 0.34 | 0.07 | 0.33 | 0.24 | 0.18 | 88.2 | 15.3 | 3.11 | 0.54 | 2.31 | 0.41 | 101 | 18 |
| 15 | 3.42 | 0.63 | 5.24 | 0.95 | 4.25 | 0.76 | 0.39 | 0.20 | 0.59 | 0.37 | 89.7 | 15.6 | 6.13 | 1.08 | 3.26 | 0.66 | 113 | 20 |
| 20 | 3.70 | 0.65 | 5.58 | 0.98 | 5.00 | 0.88 | 0.59 | 0.25 | 0.68 | 0.21 | 84.3 | 14.7 | 7.06 | 1.24 | 4.20 | 0.75 | 111 | 19 |
| 25 | 3.26 | 0.61 | 5.57 | 1.02 | 5.65 | 1.02 | 0.76 | 0.20 | 1.46 | 0.39 | 72.3 | 12.8 | 7.44 | 1.33 | 3.81 | 0.73 | 100 | 18 |
| 30 | 2.96 | 0.53 | 5.99 | 1.07 | 7.01 | 1.23 | 1.54 | 0.34 | 1.95 | 0.40 | 58.8 | 10.2 | 10.1 | 1.8 | 3.37 | 0.62 | 91.7 | 15.9 |
| 35 | 3.16 | 0.57 | 5.80 | 1.04 | 8.04 | 1.42 | 1.73 | 0.35 | 2.01 | 0.40 | 47.5 | 8.4 | 10.6 | 1.9 | 4.06 | 0.74 | 82.8 | 14.6 |
| 40 | 3.45 | 0.61 | 5.35 | 0.94 | 7.30 | 1.28 | 2.40 | 0.44 | 2.02 | 0.38 | 31.8 | 5.5 | 10.0 | 1.7 | 3.01 | 0.54 | 65.3 | 11.4 |
| 45 | 4.15 | 0.76 | 5.62 | 1.03 | 7.51 | 1.36 | 2.84 | 0.54 | 2.20 | 0.43 | 23.7 | 4.3 | 10.1 | 1.8 | 2.79 | 0.52 | 58.9 | 10.6 |
| 50 | 4.85 | 0.85 | 5.55 | 0.98 | 7.14 | 1.25 | 2.79 | 0.50 | 2.13 | 0.39 | 16.4 | 2.9 | 10.0 | 1.7 | 2.44 | 0.44 | 51.3 | 8.9 |
| 55 | 6.19 | 1.09 | 6.56 | 1.15 | 7.50 | 1.31 | 3.05 | 0.55 | 2.39 | 0.44 | 12.6 | 2.2 | 11.1 | 1.9 | 2.83 | 0.51 | 52.2 | 9.1 |
| 60 | 8.07 | 1.42 | 7.62 | 1.34 | 7.30 | 1.28 | 2.99 | 0.54 | 1.97 | 0.37 | 9.09 | 1.59 | 11.6 | 2.0 | 2.90 | 0.52 | 51.5 | 9.0 |
| 65 | 10.3 | 1.8 | 9.60 | 1.69 | 8.45 | 1.48 | 3.35 | 0.60 | 2.20 | 0.41 | 7.69 | 1.35 | 13.0 | 2.3 | 3.55 | 0.63 | 58.1 | 10.1 |
| 70 | 12.7 | 2.2 | 11.2 | 2.0 | 8.76 | 1.54 | 3.92 | 0.70 | 1.94 | 0.36 | 6.69 | 1.18 | 14.0 | 2.5 | 3.43 | 0.61 | 62.7 | 10.9 |
| 75 | 15.9 | 2.8 | 14.5 | 2.6 | 10.3 | 1.8 | 3.96 | 0.72 | 1.98 | 0.39 | 7.63 | 1.35 | 15.6 | 2.7 | 4.21 | 0.76 | 74.1 | 13.0 |
| 80 | 16.7 | 2.9 | 17.4 | 3.1 | 11.8 | 2.1 | 4.10 | 0.74 | 2.72 | 0.51 | 8.91 | 1.57 | 15.5 | 2.7 | 4.55 | 0.82 | 81.7 | 14.3 |
| 85 | 15.4 | 2.7 | 16.9 | 3.0 | 11.6 | 2.0 | 4.44 | 0.80 | 2.60 | 0.50 | 8.11 | 1.43 | 14.5 | 2.5 | 4.25 | 0.77 | 77.8 | 13.6 |
| 90 | 13.0 | 2.3 | 16.7 | 2.9 | 11.3 | 2.0 | 5.09 | 0.93 | 2.47 | 0.49 | 7.59 | 1.35 | 13.8 | 2.4 | 3.61 | 0.67 | 73.6 | 12.9 |
| 95 | 10.7 | 1.9 | 15.0 | 2.6 | 9.43 | 1.66 | 4.31 | 0.78 | 2.21 | 0.42 | 7.27 | 1.29 | 11.1 | 1.9 | 3.19 | 0.58 | 63.2 | 11.1 |
| 100 | 7.76 | 1.37 | 14.0 | 2.5 | 8.78 | 1.55 | 4.88 | 0.88 | 2.47 | 0.47 | 7.35 | 1.30 | 10.0 | 1.8 | 2.91 | 0.54 | 58.2 | 10.2 |
| 105 | 7.11 | 1.25 | 15.4 | 2.7 | 9.39 | 1.65 | 5.39 | 0.96 | 2.68 | 0.50 | 7.15 | 1.26 | 10.3 | 1.8 | 2.36 | 0.44 | 59.8 | 10.4 |
| 110 | 6.41 | 1.14 | 15.8 | 2.8 | 9.30 | 1.64 | 6.29 | 1.13 | 3.44 | 0.65 | 6.87 | 1.23 | 9.74 | 1.71 | 2.55 | 0.50 | 60.4 | 10.5 |
| 115 | 5.73 | 1.01 | 16.6 | 2.9 | 10.1 | 1.8 | 6.54 | 1.15 | 3.53 | 0.63 | 6.77 | 1.19 | 9.49 | 1.66 | 2.44 | 0.45 | 61.1 | 10.6 |
| 120 | 5.97 | 1.05 | 18.1 | 3.2 | 10.3 | 1.8 | 6.97 | 1.23 | 3.61 | 0.65 | 5.89 | 1.04 | 9.25 | 1.62 | 2.60 | 0.48 | 62.7 | 10.9 |
| 125 | 7.05 | 1.24 | 19.0 | 3.3 | 11.0 | 1.9 | 6.81 | 1.21 | 3.49 | 0.64 | 5.66 | 1.00 | 9.47 | 1.66 | 2.50 | 0.47 | 64.9 | 11.3 |
| 130 | 9.30 | 1.89 | 20.2 | 4.1 | 10.8 | 2.2 | 6.43 | 1.32 | 3.31 | 0.72 | 5.10 | 1.05 | 10.39 | 2.09 | 2.73 | 0.60 | 68.3 | 11.9 |

tical and fitting errors in the individual scattering intensities (typically 2–30 %) and the inelastic/elastic ratio error of the TOF results of LeClair and Trajmar [24] ($\approx$10%), the error on the available elastic scattering DCSs ($<$15%), the error propagated by the inelastic to elastic ratio measurements (typically 5%) and an additional error of 10% for the analyzer response function. We also include an uncertainty of 10% at $\varepsilon_0 = 10$ eV, $\approx$8% at $\varepsilon_0 = 12.5$ eV, and $>$5% at $\varepsilon = 15$ eV for the dependence of the weighted FC factors on $E_R$. We also importantly note here that no smoothing is applied to the final shape of our DCS data. Our DCSs and associated uncertainties are listed in Tables IV–XI. These DCSs are graphically compared to existing measurements and theoretical values in Figs. 3–10.

## III. SYMMETRY CONSIDERATIONS AND SELECTION RULES

Important check points (for the individual electronic excitation DCSs) regarding final products from initial electronic states of diatomic molecules can be obtained by applying symmetry rules obtained by applying group theoretical principles (Cartwright *et al.* [22], Goddard III *et al.* [23], and also Dunn [43] who applied symmetry conservation rules to breakup of diatomic molecules) to the $T$-matrix elements which are proportional to the scattering amplitudes $f_{jk}$:

$$f_{jk} \propto T_{jk} \propto \langle \Phi_j e^{ikz} | T | \Phi_k e^{ikr}/r \rangle, \tag{7}$$

where $\Phi_j$, $\Phi_k$, $e^{ikz}$, and $e^{ikr}/r$ are the wave functions of the final and initial states of the molecule and the incident (along the $z$ axis) and scattered electron, respectively. Goddard III *et al.* [23] consider various orientations of the molecule for both forward/backward scattering (axial collisions) and scattering at any other angle, but neglect the influence of rotation and vibrational or breakdown of the Born-Oppenheimer approximation [9], so that only the electronic part of the molecular wave functions are of importance in Eq. (7). Since the transition operator remains invariant under all operations of the molecular symmetry group, only $\Phi_j$, $\Phi_k$ can be affected by the reflection $\boldsymbol{\sigma}$ operator in a plane of symmetry of the molecule-plus-projectile electron system. Hence the condition

$$\boldsymbol{\sigma}[\Phi_j, \Phi_k] = -[\Phi_j, \Phi_k] \tag{8}$$

indicates that the transition is forbidden in axial collisions and this applies rigorously for $\Sigma$ states where $\Lambda = 0$. Note that for states with $\Lambda \neq 0$, there will be a component of $\Lambda$ that will cause this condition not to be satisfied. The above leads to the result that the transitions

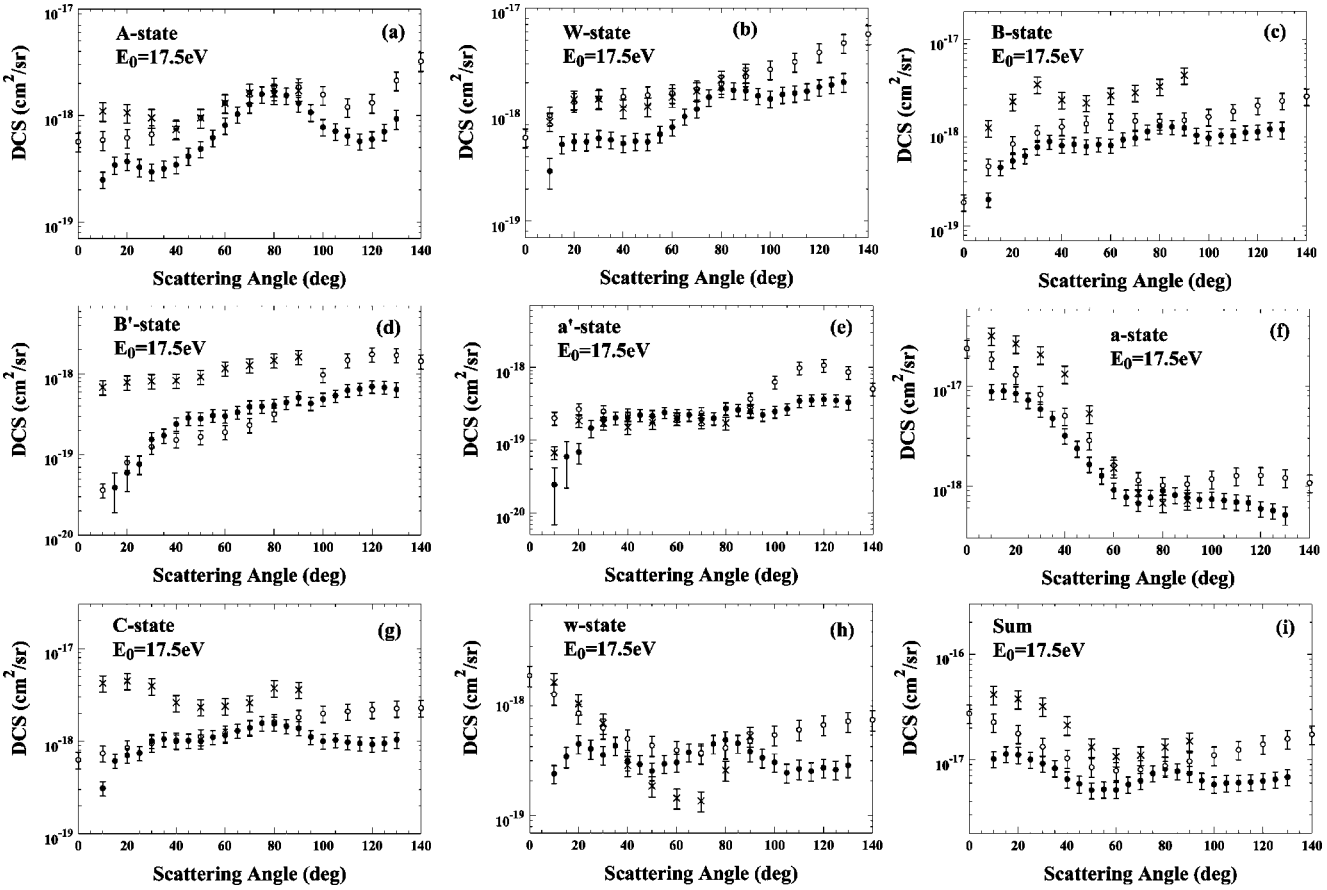


FIG. 6. Same as Fig. 5, but for $\varepsilon_0$=17.5 eV.

$$\Sigma_g^+ \leftrightarrow \Sigma_u^- \quad \text{and} \quad \Sigma_g^- \leftrightarrow \Sigma_u^+ \tag{9}$$

must go to zero for scattering angles $\theta$=0 and 180°. At other $\theta$, these transitions should be present, but weak. For orientations of the molecular axis parallel and perpendicular to the incident electron beam, the following transitions vanish (for excitation of the $\Sigma_g^+$ ground state),

$$\Sigma_g^+ \leftrightarrow \Pi_g \quad \Sigma_g^+ \leftrightarrow \Delta_u, \tag{10}$$

but are allowed for other general orientations. We can also generally expect nondipole collisions to be weaker at small scattering angles [44] and spin-exchange transitions (e.g., singlet↔triplet transitions) to show increased DCSs at larger $\theta$. The application of these symmetry rules helps us to check the observed DCS shapes that are experimentally determined. This aspect of the experiment is discussed further in the next section. For the *a* state, Lassettre [44] showed that in the region of applicability of the Born approximation (i.e., typically >10× the excitation energy, i.e., for the *a*-state excitation this would be in the region of ≈100 eV or greater, and at small $\theta$ typically <30°) the *a*-state DCSs should go to zero as $\theta \rightarrow 0°$.

Finally, two important assumptions regarding the unfolding scheme detailed above are the following:

(a) This scheme does not take into account line broadening effects of individual vibrational levels due to rotational excitation. The rotational excitation of $N_2$ by electron impact (energy losses in the range of ≈13 meV) has been investigated by Jung *et al.* [45]. They show that such dipole-forbidden excitations will dominate at low energies $\varepsilon_0$ ≈2–3 eV, which are well outside the $\varepsilon_0$ range of the present work. In this case, since the present transitions are largely forbidden (except the $X\ ^1\Sigma_g^+ \rightarrow a\ ^1\Pi_g$ excitation, which is weakly allowed), it is expected that at the present energies the above assumptions should hold reasonably well for this analysis. However, we did not observe any significant broadening in the isolated lines (e.g., of the $a\ ^1\Pi_g$ feature at small $\theta$, or of the $A\ ^3\Sigma_u^+$ features at any $\varepsilon_o$ value) to indicate rotational enhancement. This is due to our significantly lower energy resolution. Hence the present results are a sum over rotational states underlying each vibrational envelope.

(b) That it does not consider the effects of resonances (production of intermediate $N_2^-$ states). This would alter the unfolding results, but since the unfolding relies on the FC shape of the manifold as a whole, it should (on a qualitative basis) wash out such effects unless resonant excitation affected the strongest $v'$ member. This aspect of the present work is important to consider when modeling these data from a theoretical perspective. That these resonant processes are prevalent at $\varepsilon_0$<11 eV has been investigated by, e.g., Mazeau *et al.* [10] and more recently by Poparić *et al.* [21]. However, the extent to which they affect the complete electronic manifold of the low-lying states of $N_2$ (i.e., its effect over the overall unfolding of the electronic state) will

TABLE VIII. Present DCSs and associated uncertainties at $\varepsilon_0=20$ eV, units: $\times 10^{-19}$ cm$^2$/sr.

| $\theta$ (deg) | $A\,^3\Sigma_u^+$ | Error | $W\,^3\Delta_u$ | Error | $B\,^3\Pi_g$ | Error | $B'\,^3\Sigma_u^-$ | Error | $a'\,^1\Sigma_u^-$ | Error | $a\,^1\Pi_g$ | Error | $C\,^3\Pi_u$ | Error | $w\,^1\Delta_u$ | Error | Sum | Error |
|---|---|---|---|---|---|---|---|---|---|---|---|---|---|---|---|---|---|---|
| 5 | 1.47 | 0.28 | 5.03 | 0.90 | 2.45 | 0.44 | 0.07 | 0.03 | 0.01 | 0.01 | 115 | 20 | 3.19 | 0.57 | 4.10 | 0.73 | 131 | 23 |
| 10 | 1.98 | 0.38 | 5.61 | 1.01 | 4.08 | 0.73 | 0.18 | 0.11 | 0.03 | 0.01 | 130 | 23 | 4.31 | 0.77 | 4.95 | 0.89 | 151 | 26 |
| 15 | 1.80 | 0.35 | 6.41 | 1.15 | 5.44 | 0.96 | 0.36 | 0.18 | 0.06 | 0.03 | 126 | 22 | 5.84 | 1.03 | 4.07 | 0.76 | 150 | 26 |
| 20 | 1.73 | 0.34 | 6.88 | 1.22 | 7.03 | 1.23 | 0.37 | 0.18 | 0.09 | 0.05 | 112 | 19 | 6.97 | 1.23 | 4.65 | 0.85 | 140 | 24 |
| 25 | 1.54 | 0.31 | 6.30 | 1.13 | 8.50 | 1.49 | 0.74 | 0.33 | 0.21 | 0.11 | 89.6 | 15.6 | 7.87 | 1.39 | 4.37 | 0.80 | 119 | 21 |
| 30 | 2.09 | 0.40 | 5.66 | 1.02 | 9.57 | 1.68 | 1.42 | 0.38 | 0.36 | 0.12 | 70.0 | 12.2 | 8.84 | 1.55 | 5.10 | 0.93 | 103 | 18 |
| 35 | 2.23 | 0.43 | 5.34 | 0.97 | 8.87 | 1.56 | 1.57 | 0.40 | 1.03 | 0.35 | 49.0 | 8.6 | 8.10 | 1.43 | 4.64 | 0.85 | 80.7 | 14.1 |
| 40 | 3.20 | 0.59 | 5.32 | 0.96 | 9.12 | 1.61 | 1.55 | 0.35 | 1.65 | 0.36 | 33.1 | 5.8 | 8.34 | 1.48 | 3.59 | 0.66 | 65.9 | 11.5 |
| 45 | 4.27 | 0.77 | 5.00 | 0.90 | 9.11 | 1.60 | 1.98 | 0.41 | 1.42 | 0.32 | 23.6 | 4.1 | 9.39 | 1.66 | 3.39 | 0.62 | 58.1 | 10.1 |
| 50 | 5.95 | 1.06 | 5.82 | 1.04 | 8.48 | 1.50 | 1.53 | 0.33 | 1.46 | 0.32 | 15.7 | 2.8 | 9.88 | 1.74 | 3.16 | 0.58 | 52.0 | 9.1 |
| 55 | 7.27 | 1.28 | 6.32 | 1.13 | 7.81 | 1.37 | 1.95 | 0.39 | 1.07 | 0.26 | 10.6 | 1.9 | 9.30 | 1.63 | 3.29 | 0.60 | 47.6 | 8.3 |
| 60 | 8.71 | 1.54 | 11.3 | 2.0 | 7.55 | 1.33 | 2.89 | 0.55 | 1.57 | 0.34 | 7.31 | 1.30 | 9.07 | 1.60 | 2.70 | 0.50 | 51.1 | 8.9 |
| 65 | 10.0 | 1.8 | 12.2 | 2.1 | 8.81 | 1.55 | 3.16 | 0.58 | 1.37 | 0.30 | 6.59 | 1.17 | 9.63 | 1.70 | 3.00 | 0.55 | 54.8 | 9.5 |
| 70 | 12.4 | 2.2 | 15.6 | 2.7 | 10.4 | 1.8 | 4.00 | 0.74 | 1.79 | 0.37 | 7.10 | 1.26 | 8.13 | 1.44 | 2.24 | 0.44 | 61.7 | 10.7 |
| 75 | 14.2 | 2.5 | 17.1 | 3.0 | 10.1 | 1.8 | 5.15 | 0.93 | 2.02 | 0.42 | 7.74 | 1.37 | 9.30 | 1.65 | 2.58 | 0.50 | 68.2 | 11.9 |
| 80 | 11.4 | 2.0 | 20.1 | 3.5 | 9.97 | 1.76 | 6.39 | 1.17 | 2.71 | 0.56 | 8.41 | 1.50 | 9.95 | 1.76 | 2.36 | 0.49 | 71.3 | 12.4 |
| 85 | 10.5 | 1.8 | 20.2 | 3.5 | 9.49 | 1.67 | 5.77 | 1.05 | 2.19 | 0.45 | 7.88 | 1.40 | 9.14 | 1.61 | 2.29 | 0.46 | 67.5 | 11.7 |
| 90 | 9.01 | 1.59 | 18.6 | 3.3 | 8.39 | 1.48 | 4.90 | 0.89 | 1.68 | 0.35 | 6.88 | 1.22 | 7.88 | 1.39 | 2.05 | 0.40 | 59.4 | 10.3 |
| 95 | 7.35 | 1.30 | 14.0 | 2.5 | 8.58 | 1.51 | 4.20 | 0.77 | 2.14 | 0.43 | 8.62 | 1.52 | 8.01 | 1.41 | 2.04 | 0.40 | 55.0 | 9.6 |
| 100 | 7.24 | 1.29 | 12.9 | 2.3 | 8.70 | 1.53 | 4.79 | 0.88 | 1.82 | 0.39 | 8.04 | 1.42 | 8.78 | 1.55 | 2.28 | 0.45 | 54.6 | 9.5 |
| 105 | 6.00 | 1.07 | 15.4 | 2.7 | 8.94 | 1.57 | 5.12 | 0.93 | 1.51 | 0.34 | 8.58 | 1.52 | 8.20 | 1.45 | 2.50 | 0.48 | 56.3 | 9.8 |
| 110 | 5.90 | 1.05 | 17.0 | 3.0 | 8.97 | 1.57 | 5.60 | 1.01 | 2.04 | 0.41 | 8.58 | 1.51 | 8.22 | 1.45 | 2.64 | 0.50 | 59.0 | 10.3 |
| 115 | 5.38 | 0.97 | 18.5 | 3.3 | 9.98 | 1.76 | 5.95 | 1.09 | 2.29 | 0.48 | 8.09 | 1.44 | 9.60 | 1.70 | 2.04 | 0.43 | 61.8 | 10.8 |
| 120 | 6.50 | 1.16 | 19.2 | 3.4 | 10.1 | 1.8 | 6.63 | 1.19 | 2.62 | 0.52 | 7.03 | 1.25 | 8.31 | 1.47 | 2.30 | 0.46 | 62.7 | 10.9 |
| 125 | 8.23 | 1.47 | 22.0 | 3.9 | 10.7 | 1.9 | 5.88 | 1.08 | 1.83 | 0.41 | 6.57 | 1.18 | 8.66 | 1.53 | 3.09 | 0.60 | 67.0 | 11.7 |
| 130 | 11.3 | 2.0 | 24.0 | 4.2 | 11.5 | 2.0 | 6.59 | 1.20 | 2.43 | 0.51 | 5.68 | 1.03 | 7.62 | 1.35 | 2.77 | 0.55 | 71.9 | 12.5 |

certainly be less than as compared to its effect on individual vibrational levels in the same electronic state.

## IV. RESULTS AND DISCUSSIONS

All the present DCSs and their associated uncertainties are given in Tables IV–XI. These DCSs are plotted in Figs. 3–10 to show comparisons with earlier work.

(i) *$\varepsilon_0$=10 eV*: At $\varepsilon_0=10$ eV, only the *A*, *W*, and *B* states showed appreciable contributions to the energy-loss spectra and could be reliably extracted from the spectral unfolding process. These DCSs are compared to those of Cartwright *et al.* [13] and the *R*-matrix results of Gillan *et al.* [30] for the *A* state. For the *A* and *B* DCSs at large angles [Figs. 3(a) and 3(c)] we see very good agreement with the measurements of Cartwright *et al.* [13]. However, since their data is significantly lower then ours at smaller $\theta$, we suspect that the background elastic contribution would tend to lower their DCSs. The present measurements of elastic to inelastic with the moveable target source method gives more accurate results. Typically, the elastic scattering background is $\approx$40% of the elastic scattering signal at the small $\theta$, but goes down to approximately $\approx$8% at $\theta>30°$. This would explain some of the discrepancy between the Cartwright *et al.* [13] data and the present work. The difference in the two experiments is observed more clearly when we view the summed *A*, *W* and *B* DCSs in Fig. 3(d), where the effect of elastic background in the Cartwright *et al.* DCSs is evident as a strong possibility. In Fig. 3(b), our *W* state DCSs are lower than Cartwright *et al.*'s by a factor of 3 although the shapes show excellent agreement. We have also included the relative DCSs of Mazeau *et al.* [10], scaled to our results for best agreement), taken at $\varepsilon_0=9.8$ eV. These relative DCSs were obtained from their graphs and have a 10% (relative) error. For the *A*-state Fig. 3(a), shape agreement with Mazeau *et al.* and our DCSs are good. However, for the *B*-state, their DCSs show a pronounced forward scattering form that both our DCSs and those of Cartwright *et al.* do not show. This could well be associated with resonant behavior of the *B*-state which from Mazeau *et al.*'s work continues well past $\varepsilon_0=10.3$ eV (see their paper). In terms of theory, the agreement of our *A*-state DCSs with the *R*-Matrix results of Gillan *et al.* [31] [see Fig. 3(a)] needs improvement. The minimum in the theory at $\theta=80°$ is not observed by either experiment. We note that the *A*-state is the most exposed of all the electronic $N_2$ states covered here, thus (in principle) the easiest to unfold. Hence, this disagreement means largely that the theory is unable to provide accurate angular shapes.

(ii) *$\varepsilon_0$=12.5 eV*: At $\varepsilon_0=12.5$ eV, the present work covers

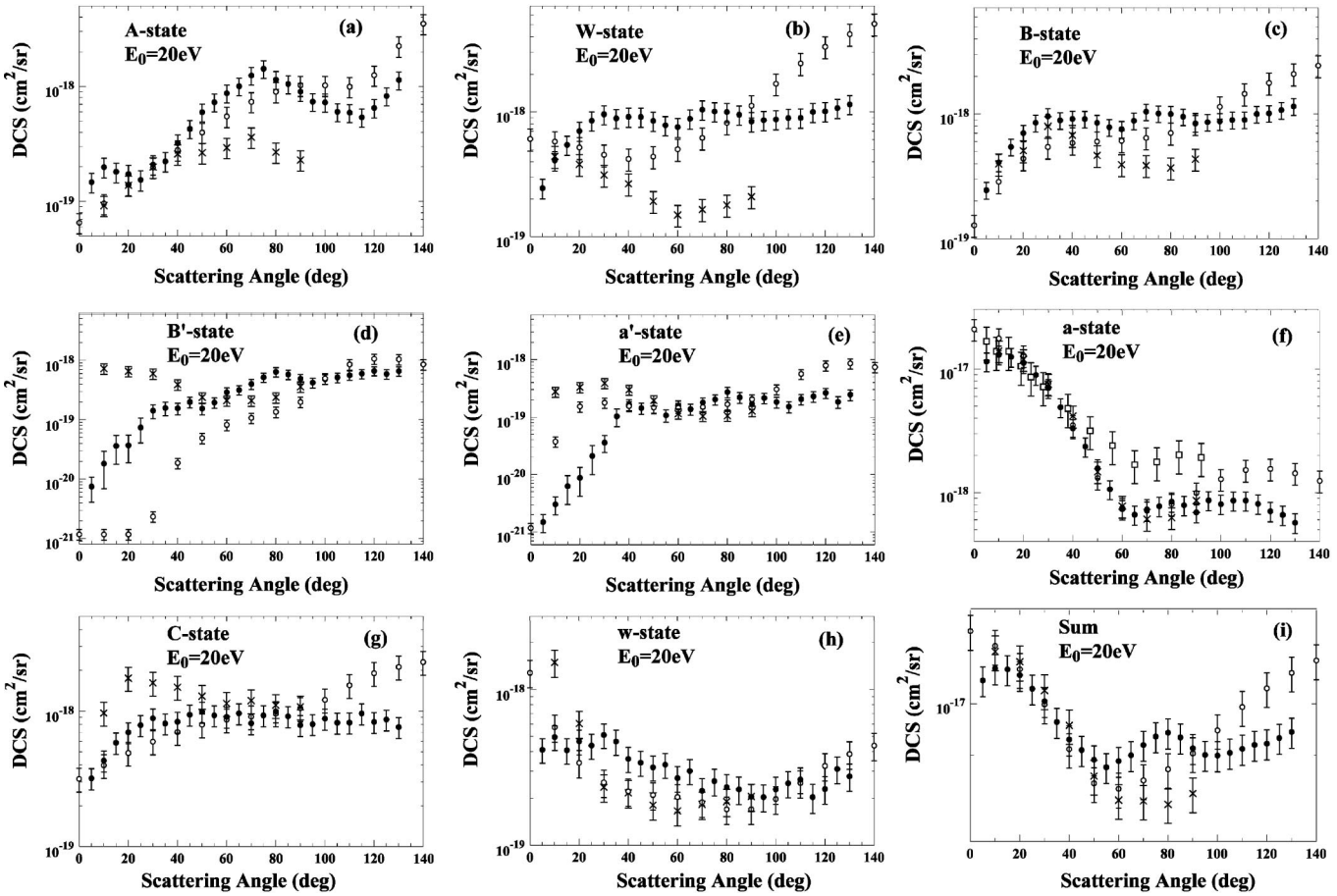


FIG. 7. Same as Fig. 5, but for $\varepsilon_0=20$ eV. Also, □, Ref. [11], relative DCSs, scaled to our results at small $\theta$.

the DCSs for all eight states. Note that the DCSs of Cartwright *et al.* [13] are multiplied by the factor 0.63 to get better agreement with ours, since in this case the shape agreement with our results is very good, especially for the summed DCSs in Fig. 4(i). This indicates that their normalization to the elastic DCS is in agreement with our results using the more elaborate moveable source method, but their spectrometer transmission correction is not. Agreement between the experiments for the *A*, *W*, and *B* states [Figs. 4(a)–4(c)] is very good, but for the $B'$, *a*, and *w* states, the agreement is surprisingly worse. The work of Cartwright *et al.* [13] does not cover the DCSs for the $a'$ and *C* states at these energies. We note that their DCSs for the excitation of the *a* state (which gives rise to the LBH bands) are in good shape agreement with ours, but disagree quantitatively by a factor of about 50%. We note the observations of both experiments regarding the fall in the *a*-state DCSs at small $\theta$, which has been discussed by Lassettre [44] using oscillator strength arguments in terms of the fact that this state has $\approx$75% magnetic dipole and 25% electric quadrupole photoemission properties. According to the Born approximation, this excitation should vanish for $\theta=0°$. In concordance with the symmetry considerations (Sec. III) above, we also find the $a'$ and $B'$ states to be the lowest DCSs in this group, and that apart from the strong small $\theta$ dependence of the *a* state, all other states display decreasing DCSs toward small $\theta$, showing consistency with the above symmetry arguments as well as (dipole) selection rules. For the *w* state [Fig. 4(h)], we note the large difference between our DCSs and those of Cartwright *et al.*, i.e., they do not observe the clear dip in our *w*-state DCSs at around 70°. We also include the relative DCSs of Mazeau *et al.* [10] for the *A* state at 12 eV [Fig. 4(a)] and the *B* state at 13 eV. Their data have been normalized to ours at large $\theta$. At this $\varepsilon_0$ value, there should be no influence of resonances for these states [10], yet both the *A* and *B* state DCSs increase at forward scattering angles, more than Cartwright *et al.*'s and the present results.

(iii) $\varepsilon_0=15$ *eV*: At this energy, there are the additional and more recent experimental DCSs of Brunger and Teubner [3] and Zetner and Trajmar [18] for comparison. In Fig. 5(a), for the *A* state, the present DCSs show an oscillatory structure with minima at $\theta=40$ and 125° and a maximum at 75°. Excellent shape agreement for this state (same figure) is observed with the results of Zetner and Trajmar [18], but disagreement at large $\theta$ is observed with the results of Cartwright *et al.* [13]. The results of Zetner and Trajmar have been scaled down by 0.45 to bring them in better agreement with ours. However, the fact that they show excellent agreement overall with the present DCSs in shape, as compared to the other measurements, may be due to their use of the same FC factors, and a similar apparatus as employed here. However, Cartwright *et al.* [13] also used the same FC factors and they are not in agreement. This raises important questions (addressed also by Brunger and Buckman [5]) as to what are

TABLE IX. Present DCSs and associated uncertainties at $\varepsilon_0=30$ eV, units: $\times 10^{-19}$ cm$^2$/sr.

| $\theta$ (deg) | $A\,^3\Sigma_u^+$ | Error | $W\,^3\Delta_u$ | Error | $B\,^3\Pi_g$ | Error | $B'\,^3\Sigma_u^-$ | Error | $a'\,^1\Sigma_u^-$ | Error | $a\,^1\Pi_g$ | Error | $C\,^3\Pi_u$ | Error | $w\,^1\Delta_u$ | Error | Sum | Error |
|---|---|---|---|---|---|---|---|---|---|---|---|---|---|---|---|---|---|---|
| 5 | 1.72 | 0.61 | 0.77 | 0.38 | 2.27 | 0.55 | 0.22 | 0.20 | 0.64 | 0.50 | 215 | 34 | 2.42 | 0.50 | 1.37 | 0.30 | 224 | 35 |
| 10 | 1.23 | 0.21 | 1.93 | 0.32 | 4.12 | 0.66 | 0.35 | 0.18 | 1.27 | 0.25 | 169 | 27 | 2.74 | 0.44 | 2.40 | 0.40 | 183 | 29 |
| 15 | 1.03 | 0.18 | 2.23 | 0.37 | 4.92 | 0.79 | 0.67 | 0.18 | 0.89 | 0.22 | 138 | 22 | 2.98 | 0.48 | 3.11 | 0.51 | 154 | 24 |
| 20 | 0.95 | 0.17 | 2.40 | 0.40 | 6.05 | 0.97 | 0.73 | 0.19 | 1.30 | 0.27 | 108 | 17 | 2.91 | 0.47 | 3.64 | 0.60 | 126 | 20 |
| 25 | 0.79 | 0.17 | 2.17 | 0.38 | 6.79 | 1.09 | 0.94 | 0.25 | 1.27 | 0.30 | 76.5 | 12.1 | 2.88 | 0.47 | 3.59 | 0.60 | 95.0 | 15.0 |
| 30 | 0.68 | 0.12 | 2.53 | 0.41 | 6.71 | 1.07 | 0.75 | 0.17 | 1.21 | 0.23 | 51.8 | 8.2 | 3.05 | 0.49 | 3.83 | 0.62 | 70.6 | 11.2 |
| 35 | 0.65 | 0.12 | 2.09 | 0.34 | 6.64 | 1.06 | 1.21 | 0.22 | 1.16 | 0.22 | 33.4 | 5.3 | 3.03 | 0.49 | 2.83 | 0.46 | 51.0 | 8.1 |
| 40 | 0.68 | 0.12 | 2.41 | 0.39 | 6.60 | 1.05 | 1.22 | 0.22 | 1.30 | 0.23 | 21.5 | 3.4 | 3.36 | 0.54 | 2.92 | 0.47 | 40.0 | 6.4 |
| 45 | 0.75 | 0.13 | 2.18 | 0.36 | 5.84 | 0.94 | 1.25 | 0.22 | 1.09 | 0.20 | 11.1 | 1.8 | 3.18 | 0.51 | 2.19 | 0.36 | 27.6 | 4.4 |
| 50 | 1.28 | 0.22 | 2.45 | 0.41 | 5.62 | 0.91 | 1.01 | 0.19 | 0.80 | 0.16 | 6.48 | 1.04 | 3.68 | 0.60 | 1.48 | 0.25 | 22.8 | 3.6 |
| 55 | 1.81 | 0.30 | 2.35 | 0.39 | 5.34 | 0.86 | 0.90 | 0.17 | 0.80 | 0.15 | 3.57 | 0.58 | 3.87 | 0.63 | 1.17 | 0.20 | 19.8 | 3.2 |
| 60 | 2.72 | 0.45 | 2.52 | 0.42 | 5.56 | 0.90 | 0.76 | 0.15 | 0.58 | 0.13 | 3.17 | 0.52 | 4.39 | 0.71 | 0.97 | 0.18 | 20.7 | 3.3 |
| 65 | 3.39 | 0.56 | 2.66 | 0.44 | 5.63 | 0.91 | 0.60 | 0.13 | 0.59 | 0.13 | 3.21 | 0.53 | 4.45 | 0.72 | 0.84 | 0.16 | 21.4 | 3.4 |
| 70 | 4.55 | 0.74 | 3.10 | 0.51 | 6.32 | 1.03 | 0.33 | 0.09 | 0.40 | 0.11 | 4.66 | 0.76 | 4.96 | 0.80 | 0.85 | 0.16 | 25.2 | 4.0 |
| 75 | 5.12 | 0.83 | 3.48 | 0.57 | 7.11 | 1.14 | 0.37 | 0.11 | 0.41 | 0.11 | 5.75 | 0.93 | 5.57 | 0.90 | 0.96 | 0.17 | 28.8 | 4.6 |
| 80 | 6.06 | 0.98 | 4.23 | 0.69 | 7.82 | 1.26 | 0.60 | 0.14 | 0.47 | 0.12 | 7.34 | 1.18 | 4.95 | 0.80 | 1.14 | 0.20 | 32.6 | 5.2 |
| 85 | 6.30 | 1.02 | 5.05 | 0.82 | 8.37 | 1.34 | 0.83 | 0.18 | 0.73 | 0.16 | 8.35 | 1.34 | 4.94 | 0.80 | 1.21 | 0.22 | 35.8 | 5.7 |
| 90 | 6.44 | 1.04 | 5.92 | 0.96 | 8.84 | 1.42 | 1.10 | 0.22 | 1.04 | 0.21 | 9.36 | 1.50 | 4.81 | 0.78 | 1.26 | 0.23 | 38.8 | 6.2 |
| 95 | 5.92 | 0.96 | 6.22 | 1.01 | 8.99 | 1.44 | 1.59 | 0.31 | 1.07 | 0.23 | 9.81 | 1.58 | 5.40 | 0.88 | 1.68 | 0.30 | 40.7 | 6.5 |
| 100 | 4.86 | 0.79 | 7.14 | 1.15 | 9.03 | 1.45 | 1.93 | 0.34 | 1.33 | 0.25 | 9.75 | 1.56 | 5.42 | 0.87 | 1.86 | 0.32 | 41.3 | 6.6 |
| 105 | 4.58 | 0.74 | 7.56 | 1.22 | 8.89 | 1.42 | 3.17 | 0.53 | 2.04 | 0.35 | 8.82 | 1.41 | 5.75 | 0.93 | 1.42 | 0.26 | 42.2 | 6.7 |
| 110 | 3.55 | 0.58 | 7.91 | 1.27 | 9.22 | 1.47 | 3.24 | 0.55 | 2.28 | 0.40 | 8.79 | 1.41 | 5.75 | 0.93 | 1.69 | 0.31 | 42.4 | 6.7 |
| 115 | 3.52 | 0.57 | 8.03 | 1.29 | 9.75 | 1.56 | 4.23 | 0.69 | 2.35 | 0.40 | 8.42 | 1.35 | 6.65 | 1.07 | 1.24 | 0.23 | 44.2 | 7.0 |
| 120 | 3.50 | 0.57 | 8.89 | 1.43 | 10.1 | 1.6 | 4.09 | 0.68 | 2.64 | 0.45 | 8.23 | 1.32 | 6.30 | 1.01 | 1.37 | 0.26 | 45.1 | 7.2 |
| 125 | 5.12 | 0.83 | 9.31 | 1.49 | 11.7 | 1.9 | 4.71 | 0.77 | 2.78 | 0.47 | 8.09 | 1.30 | 7.02 | 1.13 | 1.09 | 0.22 | 49.8 | 7.9 |
| 130 | 7.42 | 1.19 | 9.38 | 1.50 | 13.4 | 2.1 | 4.32 | 0.71 | 2.77 | 0.47 | 8.41 | 1.35 | 7.07 | 1.13 | 1.20 | 0.24 | 54.0 | 8.6 |

the major factors that cause disagreements between various measurements. This is later addressed in Sec. V. The DCSs of Brunger and Teubner [3] show disagreement with our results. Agreement with the *R*-matrix results [32] [Fig. 5(a)] is poor, with a theoretical angular behavior that is almost opposite to the experimental values. For the *W*, *B*, and *a* DCSs [Figs. 5(b), 5(c), and 5(f)] we observe excellent agreement with the DCSs of Zetner and Trajmar [18] (again scaled down by 0.45), but some disagreement at large $\theta$ with Cartwright *et al.* DCSs and overall disagreement with the DCSs of Brunger and Teubner [3] except for the *a*-state DCSs [Fig. 5(f)] where the shape agreement with the DCSs of Brunger and Teubner is excellent (but their data would need to be scaled down by $\approx$0.33 to bring them in quantitative agreement with our results). For the *a*-state DCSs we observe large $\theta$ disagreement with the DCSs of Cartwright *et al.* Based on similar observations for the summed DCSs [Fig. 5(i)], we conclude that their normalization to the elastic cross section may have been over estimated for $\theta>80°$. For this state, we also observe a small drop in DCSs at $\theta>20°$. Again we note the drop in the DCSs for the $B'$, $a'$, *B*, *W*, and *C* state DCSs toward small $\theta$. Overall agreement with theory is poor. For the summed DCSs [Fig. 5(i)] the DCSs of Zetner and Trajmar [18] are lower than ours because they do not include the other $a'$, $B'$, *C*, and *w* states. Finally, the fact that we observe excellent shape agreement with Zetner and Trajmar [18], indicates that our unfolding of the $N_2$ spectrum and the elastic normalization to be consistent with theirs. Zetner and Trajmar properly accounted for their elastic backgrounds by diverting the gas into the scattering chamber via a side leak. However, their analyzer response correction is not as reliable as ours which uses the more accurate TOF DCSs of LeClair and Trajmar [24].

(iv) *$\varepsilon_0$=17.5 eV*: Agreement with earlier measurements of Brunger and Teubner [3] and Cartwright *et al.* [13] is mixed [Figs. 6(a)–6(i)]. At small angles we see generally good agreement for the *A*, *B*, $B'$, $a'$, *a*, and *C* states, however, at large $\theta$, there is disagreement where the DCSs of Cartwright *et al.* are higher. Figure 6(i) shows the summed DCSs are in reasonable shape agreement, but the Cartwright *et al.* DCSs are significantly higher than ours at $\theta>90°$. We note the pronounced oscillatory shape of the *A*- and *w*-state DCSs which resembles those observed at $\varepsilon_0=15$ eV. All the DCSs decrease as they approach forward scattering supporting the discussion in Sec. III regarding symmetry rules. Note that the maximum in the *a*-state DCSs is at $\theta\approx15°$ at this $\varepsilon_0$ value.

(v) *$\varepsilon_0$=20 eV*: Here (see Fig. 7), the summed DCSs show good agreement at $\theta<60°$, but diverge at larger $\theta$. Our results show a more gradual decrease in the DCSs for the $a'$

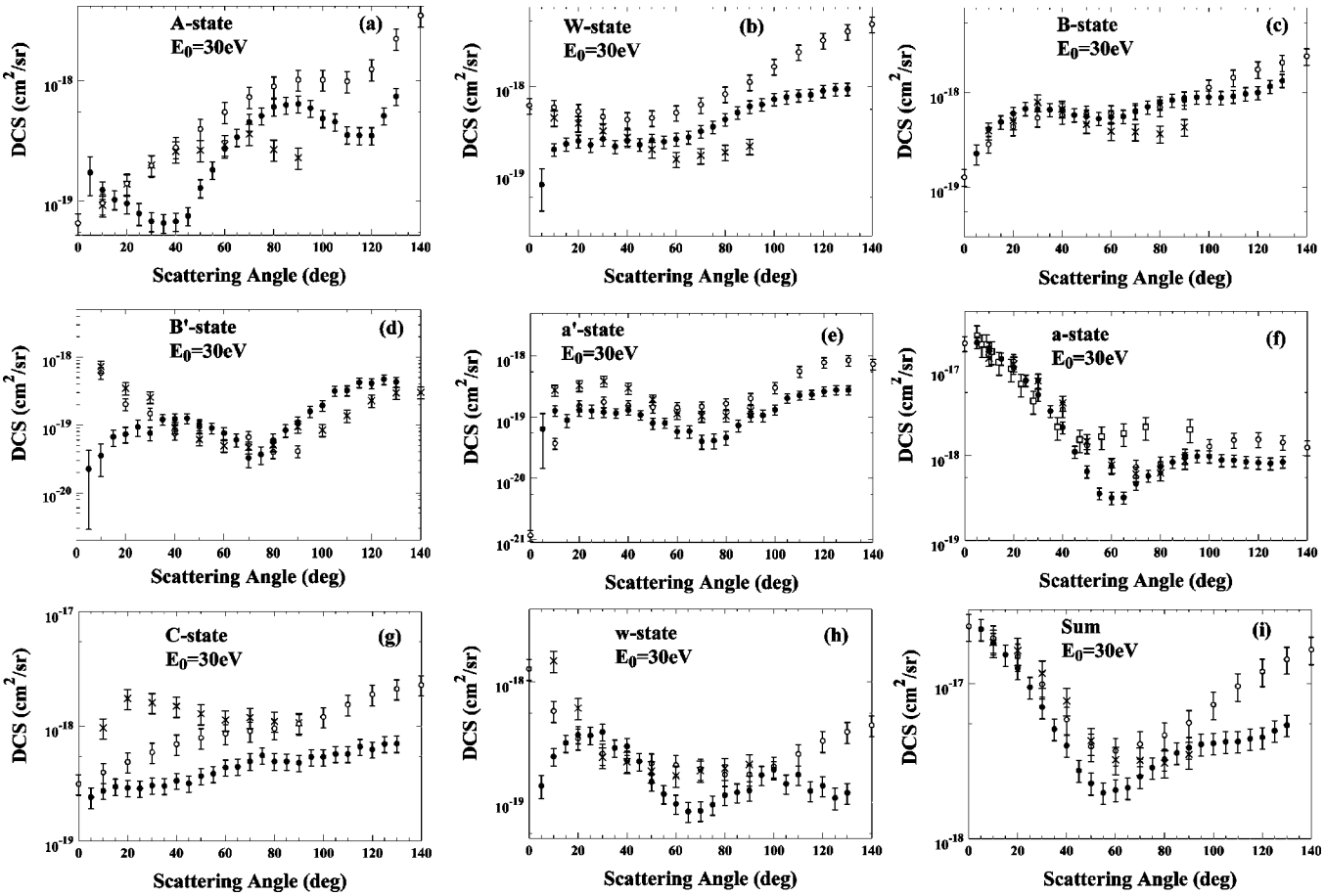


FIG. 8. Same as Fig. 7, but for $\varepsilon_0=30$ eV.

and $B'$ excitations than Cartwright *et al.* We note that Brunger and Teubner's DCSs for the $B'$ state rise towards smaller $\theta$, in disagreement with the symmetry arguments in Sec. III. Also, the shape agreement with Cartwright *et al.*'s DCS values is better than that of Brunger and Teubner, except for the *a* state where agreement with them and ours is excellent. The DCSs of Cartwright *et al.* rise above ours [see Fig. 7(i), for the summed DCSs] at $\theta>90°$. We note the maximum in the *a*-state DCSs moving closer to smaller $\theta$ as $\varepsilon_0$ increases. In this case the maximum is at $\theta=10°$. This is in rough agreement with the generalized oscillator strength measurements of the excitation of the *a* state [44]. At this $\varepsilon_0$ value we also include for comparison the *a*-state relative DCSs of Finn and Doering [11], which have been normalized to the experimental DCSs at $\theta\approx20°$. Their measurements were performed with a significantly lower energy resolution of 120 meV (FWHM) and hence their spectrometer was not able to resolve the contribution of the other states to the *a*-state DCS (*A*–*W* states; see Table I for the energy-loss values of these states). However, their results clearly demonstrate the dominance of the *a*-state DCS as far as forward scattering (at angles below 40°) is concerned. Above 40°, their DCSs are increased because of the additional contribution of the *A*–*W* states, not including the *C* state. This increase is observed also at other $\varepsilon_0$ values and implies that their integrated cross sections for the *a* state are too high at larger $\theta$ because of contributions from other states in the same energy-loss region (see also *a*-state DCSs figures at higher $\varepsilon_0$ values)

(vi) $\varepsilon_0=30$ *eV*: We observe similar trends (Fig. 8) to those at $\varepsilon_0=20$ eV, except that the *a* state shows a pronounced dip at $\theta=60°$, and we are not able to locate a minimum in the *a*-state excitation DCSs at small $\theta$ as expected by the generalized oscillator strength picture of Lassettre [44]. We also note the striking oscillatory behavior of the *A*- and *w*-state DCSs that is not observed by the earlier measurements. This could be due to normalization to the available elastic DCSs at these small $\theta$ values, which may be subject to background problems. We intend to do future checks using the moveable target method at these small $\theta$ and higher $\varepsilon_0$ values, where the contribution of the *a* state to the energy-loss spectrum is dominant, i.e., >90%.

(vii) $\varepsilon_0=50$ *eV*: Here, the summed DCSs [Fig. 9(i)] are in best agreement with other measurements, even at large $\theta$. However, the individual DCSs show disagreement especially for the *B* state or the *A* state and the *C* state. In most cases, averaged over all $\theta$, quantitative agreement is reasonable, but shape disagreements occur usually at large $\theta$, except for the *B*-state DCSs which are in excellent agreement for $\theta>30°$. It is important to note that at small $\theta$, since the *a* state dominates the energy-loss spectrum, its contribution accumulates quickly with excellent statistics. However, to obtain a statistically significant spectrum which enables one to unfold the other states' contributions, typically 30–50 times more real

TABLE X. Present DCSs and associated uncertainties at $\varepsilon_0=50$ eV, units: $\times 10^{-19}$ cm$^2$/sr.

| $\theta$ (deg) | $A\,^3\Sigma_u^+$ | Error | $W\,^3\Delta_u$ | Error | $B\,^3\Pi_g$ | Error | $B'\,^3\Sigma_u^-$ | Error | $a'\,^1\Sigma_u^-$ | Error | $a\,^1\Pi_g$ | Error | $C\,^3\Pi_u$ | Error | $w\,^1\Delta_u$ | Error | Sum | Error |
|---|---|---|---|---|---|---|---|---|---|---|---|---|---|---|---|---|---|---|
| 5 | 0.84 | 0.14 | 0.52 | 0.10 | 1.30 | 0.21 | 0.13 | 0.09 | 0.16 | 0.10 | 203 | 32 | 1.48 | 0.24 | 1.32 | 0.23 | 209 | 33 |
| 10 | 1.02 | 0.17 | 0.49 | 0.10 | 1.23 | 0.20 | 0.18 | 0.08 | 0.20 | 0.10 | 166 | 26 | 1.50 | 0.24 | 2.26 | 0.37 | 173 | 27 |
| 15 | 1.40 | 0.23 | 0.61 | 0.11 | 1.40 | 0.23 | 0.34 | 0.10 | 0.39 | 0.12 | 119 | 19 | 1.62 | 0.26 | 3.30 | 0.53 | 128 | 20 |
| 20 | 1.65 | 0.27 | 0.73 | 0.13 | 1.53 | 0.25 | 0.51 | 0.12 | 0.51 | 0.13 | 82.2 | 13.0 | 1.89 | 0.30 | 3.87 | 0.62 | 92.8 | 14.7 |
| 25 | 1.76 | 0.29 | 0.94 | 0.17 | 1.74 | 0.28 | 0.76 | 0.15 | 0.86 | 0.17 | 53.7 | 8.5 | 2.07 | 0.33 | 3.86 | 0.62 | 65.7 | 10.4 |
| 30 | 1.89 | 0.31 | 1.10 | 0.19 | 1.74 | 0.28 | 0.71 | 0.14 | 0.77 | 0.16 | 28.4 | 4.5 | 1.95 | 0.31 | 3.18 | 0.51 | 39.7 | 6.3 |
| 35 | 1.78 | 0.29 | 1.21 | 0.21 | 1.77 | 0.29 | 0.71 | 0.14 | 0.84 | 0.16 | 16.3 | 2.6 | 1.89 | 0.30 | 2.88 | 0.47 | 27.4 | 4.4 |
| 40 | 1.49 | 0.25 | 1.48 | 0.25 | 2.15 | 0.35 | 0.60 | 0.14 | 0.76 | 0.16 | 9.84 | 1.57 | 1.87 | 0.30 | 2.44 | 0.40 | 20.6 | 3.3 |
| 45 | 1.33 | 0.22 | 1.78 | 0.30 | 2.22 | 0.36 | 0.75 | 0.15 | 0.59 | 0.12 | 4.81 | 0.77 | 1.91 | 0.31 | 1.73 | 0.29 | 15.1 | 2.4 |
| 50 | 1.50 | 0.25 | 1.88 | 0.31 | 2.43 | 0.40 | 0.74 | 0.15 | 0.49 | 0.11 | 3.55 | 0.58 | 1.89 | 0.31 | 1.38 | 0.23 | 13.9 | 2.2 |
| 55 | 1.42 | 0.24 | 2.18 | 0.36 | 2.43 | 0.40 | 0.62 | 0.13 | 0.67 | 0.13 | 3.14 | 0.51 | 1.83 | 0.30 | 0.76 | 0.14 | 13.0 | 2.1 |
| 60 | 1.69 | 0.28 | 1.88 | 0.31 | 2.01 | 0.33 | 0.44 | 0.10 | 0.46 | 0.10 | 2.98 | 0.49 | 1.76 | 0.29 | 0.49 | 0.10 | 11.7 | 1.9 |
| 65 | 2.18 | 0.36 | 2.28 | 0.38 | 2.25 | 0.37 | 0.36 | 0.09 | 0.43 | 0.10 | 3.20 | 0.52 | 1.90 | 0.31 | 0.21 | 0.07 | 12.8 | 2.1 |
| 70 | 3.09 | 0.51 | 2.49 | 0.41 | 2.50 | 0.41 | 0.36 | 0.10 | 0.42 | 0.10 | 3.57 | 0.58 | 1.91 | 0.31 | 0.27 | 0.07 | 14.6 | 2.4 |
| 75 | 3.21 | 0.53 | 2.52 | 0.42 | 2.83 | 0.47 | 0.30 | 0.10 | 0.51 | 0.11 | 3.73 | 0.61 | 2.41 | 0.39 | 0.30 | 0.08 | 15.8 | 2.6 |
| 80 | 3.37 | 0.56 | 2.58 | 0.43 | 3.25 | 0.53 | 0.25 | 0.09 | 0.41 | 0.10 | 3.61 | 0.59 | 2.32 | 0.38 | 0.36 | 0.09 | 16.2 | 2.6 |
| 85 | 2.88 | 0.48 | 2.48 | 0.42 | 2.79 | 0.46 | 0.45 | 0.11 | 0.49 | 0.11 | 3.01 | 0.50 | 2.28 | 0.38 | 0.29 | 0.08 | 14.7 | 2.4 |
| 90 | 2.47 | 0.41 | 2.99 | 0.50 | 3.33 | 0.55 | 0.66 | 0.14 | 0.59 | 0.13 | 2.95 | 0.49 | 2.64 | 0.43 | 0.46 | 0.10 | 16.1 | 2.6 |
| 95 | 2.00 | 0.34 | 3.21 | 0.53 | 3.66 | 0.60 | 0.93 | 0.18 | 0.65 | 0.14 | 2.91 | 0.48 | 2.91 | 0.48 | 0.50 | 0.11 | 16.8 | 2.7 |
| 100 | 1.40 | 0.24 | 2.59 | 0.43 | 3.55 | 0.58 | 1.29 | 0.23 | 0.78 | 0.16 | 2.79 | 0.46 | 2.75 | 0.45 | 0.61 | 0.12 | 15.8 | 2.5 |
| 105 | 1.39 | 0.24 | 2.89 | 0.48 | 3.43 | 0.56 | 1.67 | 0.29 | 0.81 | 0.16 | 2.90 | 0.48 | 2.80 | 0.46 | 0.52 | 0.11 | 16.4 | 2.6 |
| 110 | 1.25 | 0.22 | 3.17 | 0.52 | 3.62 | 0.59 | 1.71 | 0.30 | 0.87 | 0.17 | 2.97 | 0.49 | 2.92 | 0.47 | 0.44 | 0.11 | 17.0 | 2.7 |
| 115 | 1.76 | 0.30 | 3.67 | 0.60 | 3.71 | 0.60 | 1.78 | 0.31 | 1.08 | 0.20 | 3.40 | 0.56 | 3.00 | 0.49 | 0.59 | 0.13 | 19.0 | 3.0 |
| 120 | 2.42 | 0.40 | 3.76 | 0.62 | 4.18 | 0.68 | 2.08 | 0.35 | 0.85 | 0.17 | 3.94 | 0.64 | 2.79 | 0.45 | 0.66 | 0.14 | 20.7 | 3.3 |
| 125 | 3.28 | 0.54 | 4.13 | 0.68 | 4.43 | 0.72 | 1.87 | 0.32 | 0.82 | 0.17 | 4.40 | 0.71 | 2.97 | 0.48 | 0.66 | 0.14 | 22.6 | 3.6 |
| 130 | 4.73 | 0.77 | 3.82 | 0.62 | 4.81 | 0.78 | 1.79 | 0.31 | 0.69 | 0.15 | 4.57 | 0.74 | 2.72 | 0.44 | 0.58 | 0.12 | 23.7 | 3.8 |

time is required to get adequate statistics. The agreement for the *a*-state DCSs is excellent, except our results show clear undulating structure at $\theta > 50°$. In conjunction with the previous $\varepsilon_0$ data, the DCSs for excitation of this state, shows clear nondipole-type behavior that is not picked up by the earlier data. A pronounced oscillatory structure is again observed for the *A*-state DCSs, which show a double maximum-minimum structure, in some agreement with Cartwright *et al.* Such a structure is useful in testing theoretical models to gauge the accuracy of the wave functions as well as collision dynamics for modeling the electron impact excitation of this important state.

(viii) $\varepsilon_0 = 100$ *eV*: Here, we can only compare with the DCSs for excitation of the *a* state of Finn and Doering [11]. We have normalized their DCSs to ours at small $\theta$. Again, we see the increased contribution from the metastable states in the energy region of the *a* state as discussed in, e.g., Sec. III (v) above. The $B'$ state's DCSs display a minimum at $\theta = 80°$.

## V. CONCLUSIONS

We have presented a large range of experimental low-energy electron scattering DCSs for the excitation of the $N_2$ $A\,^3\Sigma_u^+$, $B\,^3\Pi_g$, $W\,^3\Delta_u$, $B\,^3\Sigma_u^-$, $a\,^1\Sigma_u^-$, $a\,^1\Pi_g$, $w\,^1\Delta_u$, and $C\,^3\Pi_u$ electronic states, and find excellent shape agreement between these measurements and those of Zetner and Trajmar [18], but mixed agreements with the results of Cartwright *et al.* [13] and Brunger and Teubner [3] are observed. There are several factors that could result in such disagreements:

(i) Normalization of inelastic DCSs to the elastic DCSs for $N_2$: Whereas the available elastic scattering DCSs for $N_2$ are in good agreement (typically within 12%), normalizing to them is made difficult, especially at small $\theta$, because of background effects produced by elastically scattered secondary electrons from surfaces in the apparatus, which increase at small $\theta$ when the detector provides an additional target for the incident electron beam. The present work accounts for this by using a recently developed moveable target source method [34] and consequently should provide significantly improved results.

(ii) Transmission of the electron spectrometer for different $E_R$ electrons: This was corrected by using the most recent TOF experimental data of LeClair and Trajmar [24] and should therefore provide very accurate absolute DCSs. In addition, the spectrometer used was tuned (using the TOF data) so that the entire energy-loss range of the spectrum had a constant transmission within 10% (this is the relative accu-

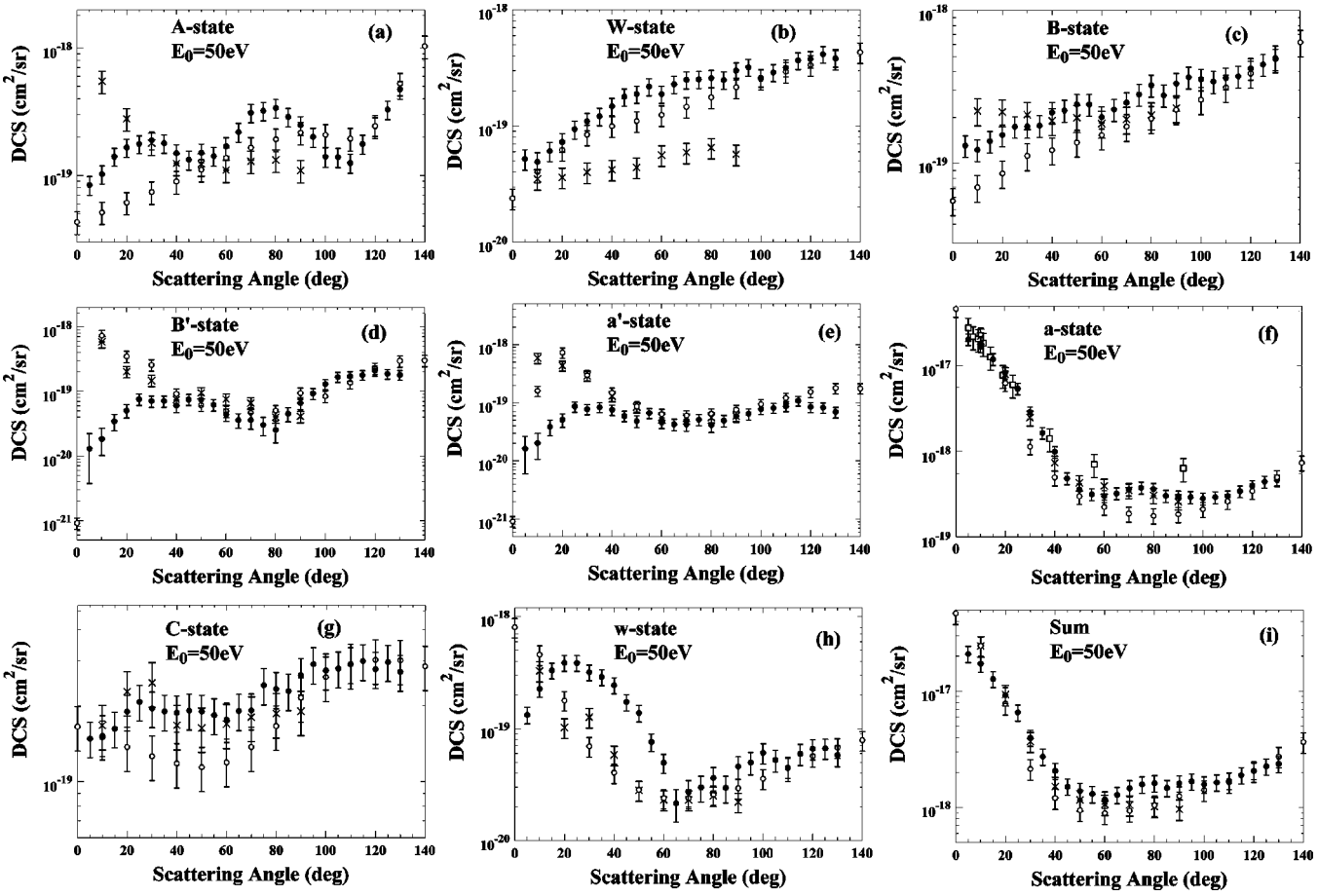


FIG. 9. Same as Fig. 7, but for $\varepsilon_0 = 50$ eV.

racy of the TOF data of LeClair and Trajmar). The transmission was stabilized by baking both the analyzer and the electron gun within a clean vacuum (maintained by incorporating a Diffstack™ diffusion pump with a constant double-stage Freon™ diffusion pump oil baffle that operated at near liquid-nitrogen temperatures). The fact that our electron beam apparatus was able to perform stably for several weeks before needing minor adjustments to tuning the electron gun, and running constantly over a period of one year before servicing for cleaning attests to this.

(iii) Reliability and consistency of individual electronic-vibrational excitation energies and FC factors: We strongly recommend that in this type of work that FC factors be tabulated so that future experimental work is able to make a

TABLE XI. Present DCSs and associated uncertainties at $\varepsilon_0 = 100$ eV, units: $\times 10^{-19}$ cm$^2$/sr.

| $\theta$ (deg) | $A\,^3\Sigma_u^+$ | Error | $W\,^3\Delta_u$ | Error | $B\,^3\Pi_g$ | Error | $B'^3\Sigma_u^-$ | Error | $a'^1\Sigma_u^-$ | Error | $a\,^1\Pi_g$ | Error | $C\,^3\Pi_u$ | Error | $w\,^1\Delta_u$ | Error | Sum | Error |
|---|---|---|---|---|---|---|---|---|---|---|---|---|---|---|---|---|---|---|
| 10 | 0.43 | 0.07 | 0.27 | 0.05 | 0.47 | 0.08 | 0.12 | 0.06 | 0.24 | 0.08 | 140 | 22 | 0.55 | 0.09 | 4.02 | 0.64 | 146 | 23 |
| 20 | 1.14 | 0.19 | 0.53 | 0.10 | 0.59 | 0.10 | 0.50 | 0.09 | 0.79 | 0.16 | 49.7 | 7.9 | 1.17 | 0.19 | 5.81 | 0.93 | 60.3 | 9.6 |
| 30 | 1.25 | 0.20 | 0.56 | 0.10 | 0.73 | 0.12 | 0.30 | 0.07 | 0.57 | 0.11 | 12.2 | 2.0 | 1.11 | 0.18 | 3.38 | 0.55 | 20.1 | 3.2 |
| 40 | 0.95 | 0.16 | 0.71 | 0.12 | 0.63 | 0.11 | 0.23 | 0.06 | 0.25 | 0.07 | 3.34 | 0.54 | 0.84 | 0.14 | 1.49 | 0.25 | 8.45 | 1.37 |
| 50 | 0.90 | 0.15 | 0.89 | 0.15 | 0.60 | 0.10 | 0.27 | 0.07 | 0.40 | 0.08 | 1.90 | 0.31 | 0.86 | 0.15 | 0.35 | 0.07 | 6.17 | 1.00 |
| 60 | 0.69 | 0.12 | 0.68 | 0.12 | 0.41 | 0.07 | 0.15 | 0.04 | 0.19 | 0.05 | 1.12 | 0.19 | 0.49 | 0.08 | 0.20 | 0.04 | 3.93 | 0.64 |
| 70 | 0.75 | 0.13 | 0.49 | 0.09 | 0.40 | 0.07 | 0.048 | 0.032 | 0.16 | 0.04 | 0.77 | 0.13 | 0.40 | 0.07 | 0.10 | 0.03 | 3.12 | 0.52 |
| 80 | 0.61 | 0.11 | 0.45 | 0.08 | 0.38 | 0.07 | 0.022 | 0.014 | 0.09 | 0.04 | 0.73 | 0.13 | 0.38 | 0.07 | 0.19 | 0.05 | 2.84 | 0.47 |
| 90 | 0.66 | 0.12 | 0.61 | 0.11 | 0.60 | 0.11 | 0.093 | 0.042 | 0.14 | 0.05 | 0.69 | 0.12 | 0.28 | 0.05 | 0.18 | 0.05 | 3.27 | 0.55 |
| 100 | 0.51 | 0.09 | 0.53 | 0.10 | 0.65 | 0.11 | 0.21 | 0.05 | 0.14 | 0.05 | 0.72 | 0.13 | 0.17 | 0.03 | 0.21 | 0.05 | 3.14 | 0.52 |
| 110 | 0.55 | 0.10 | 0.66 | 0.12 | 0.59 | 0.11 | 0.25 | 0.06 | 0.13 | 0.05 | 0.84 | 0.15 | 0.21 | 0.04 | 0.19 | 0.05 | 3.41 | 0.57 |
| 120 | 0.60 | 0.11 | 0.83 | 0.15 | 0.52 | 0.10 | 0.30 | 0.08 | 0.13 | 0.06 | 1.00 | 0.18 | 0.26 | 0.05 | 0.15 | 0.05 | 3.78 | 0.63 |
| 130 | 0.66 | 0.13 | 0.50 | 0.11 | 0.36 | 0.08 | 0.31 | 0.09 | 0.13 | 0.07 | 1.40 | 0.24 | 0.26 | 0.05 | 0.05 | 0.03 | 3.67 | 0.61 |

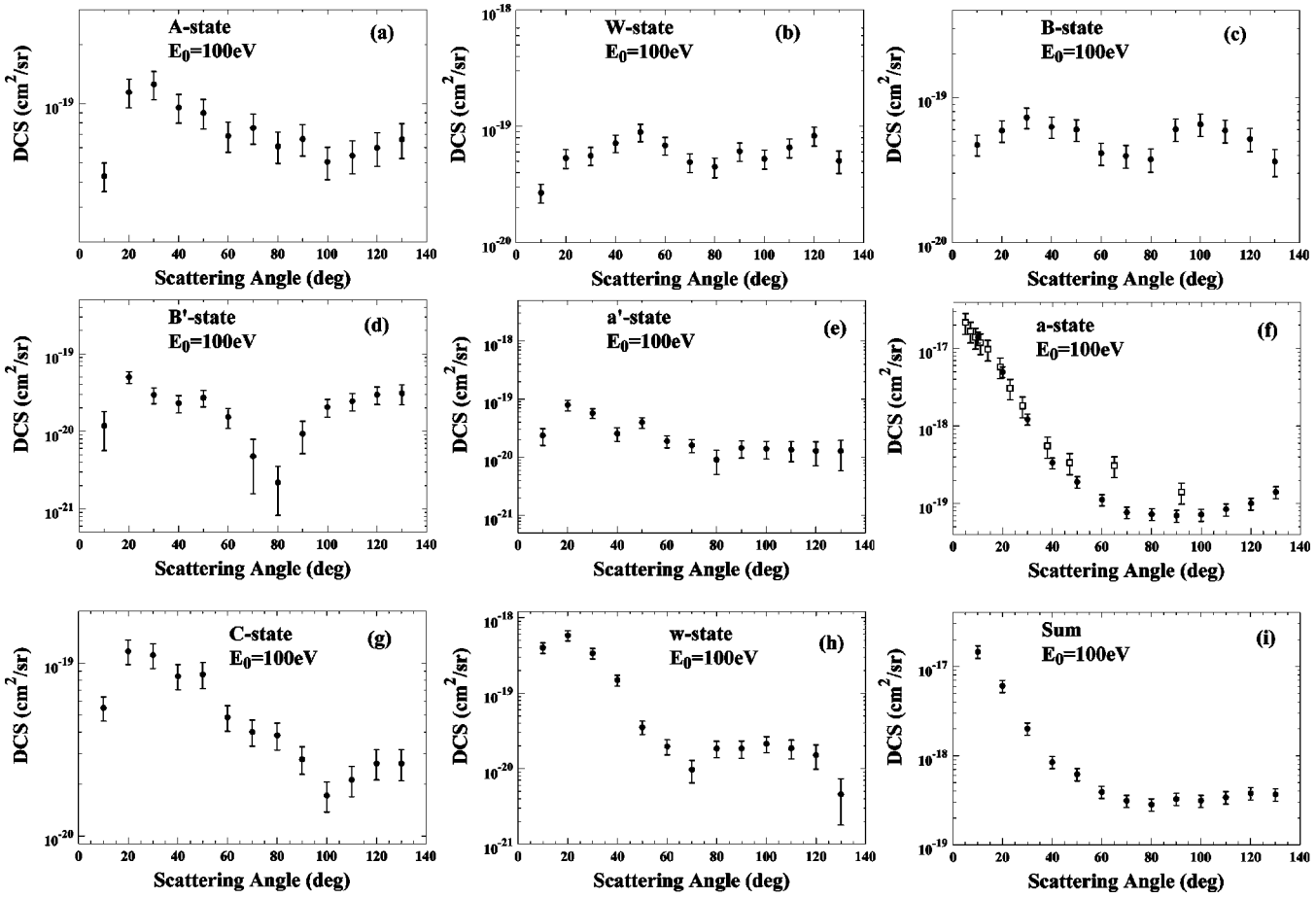


FIG. 10. Same as Fig. 7, but for $\varepsilon_0 = 100$ eV.

systematic comparison with existing measurements so that deviations can be clearly interpreted. In this area of $N_2$ (in contrast to higher-lying energy loss values [46] there are insignificant perturbative interactions between electronic potentials, so FC factors should be consistent and accurate. Comparison of our compilation with those semiempirically derived by Gilmore *et al.* [39], based on spectroscopic data, gives very good agreement. These FC factors give reasonable fits to the energy-loss spectra with low $\chi_\nu^2$ value in the range typically below 3 and provided relative fractions with errors below 15% in most cases. We have tabulated these factors so that future measurements can critically compare with ours.

(iv) Linearity of the energy-loss scale: The linearity of the energy-loss scale (determined by the energy-loss ramp; in our case obtained by a 12-bit 0–10 V digital-to-analog converter) gave a linearity within ±0.002 V over the 10 V range, as was checked using an accurate digital voltmeter. This is adequate given the resolution of our experiment (33–40 meV).

(v) Flux-weighted FC factors: An important factor in unfolding low-energy spectra in which $\Delta E_R$, the change of the residual electron energy across an entire electronic manifold, becomes a significant fraction of the mean $E_R$ across the manifold (typically $<0.2$) it is necessary to consider the effect of the excitation function which will affect (enhance) the lower energy loss vibrational levels [19]. The use of flux-weighted FC factors alleviates this problem, but should include an additional electronic excitation function for improved accuracy. This, however, requires a theoretical calculation as a guide.

The present work should result in an improvement of the experimental picture regarding electron scattering from $N_2$ over a large energy range. Unfortunately, there is a paucity of theoretical data, and the only theory available (viz. the *R* matrix of Gillan *et al.* [31]) does not seem to be reliable at the DCS level. Reliable theoretical models to establish the accuracy of the FC fitting methods used to analyze the electron energy-loss spectra are badly needed at this stage. We also recommend that FC factors and energy levels be published by both theoretical and experimental investigations, as a check of methods used. For theory, this serves to display the accuracy of wave functions used, whereas for experiment it allows one to check consistency between the different experiments. This is required in an effort to solve long-overdue problems when comparing different investigations. It is hoped that this work will encourage more research regarding electron-$N_2$ excitation DCSs in the near future. We intend to extend the present investigations to look at the less well-characterized higher levels in the energy-loss region of 11–14.5 eV where perturbative interactions between the higher-lying Rydberg series (e.g., the $^1\Pi_g$ states) complicate the picture, but also provide some very fruitful physics.

**ACKNOWLEDGMENTS**

The research carried out at the Jet Propulsion Laboratory, California Institute of Technology was sponsored by the National Aeronautics and Space Administration. Financial support through NASA's Planetary Atmospheres program is gratefully acknowledged. The work carried out at California State University, Fullerton was funded by the National Science Foundation under Grant No. NSF-PHY-RUI-0096808. Mr. Patrick Yan participated in this project under the Troy Tech internship program. We also acknowledge the development of the spectrum unfolding software by CSUF Physics undergraduate students D. Mathews and G. Mikaelian. Contributions by Dr. Russ Laher (Caltech) regarding the $N_2$ FC factors are very gratefully acknowledged. Discussions with Dr. J. W. McConkey are gratefully acknowledged. Finally, we thank Dr. C. P. Malone for his assistance in preparation of the final manuscript.

[1] S. Trajmar, D. F. Register, and A. Chutjian, Phys. Rep. **97**, 219 (1983).
[2] Y. Itikawa, M. Hayashi, A. Ichimura, K. Onda, M. Nakamura, H. Nishimura, and T. Takayanagi, J. Phys. Chem. Ref. Data **15**, 985 (1986).
[3] M. J. Brunger and P. J. O. Teubner, Phys. Rev. A **41**, 1413 (1990).
[4] T. Majeed and D. J. Strickland, J. Phys. Chem. Ref. Data **26**, 335 (1997).
[5] M. J. Brunger and S. J. Buckman, Phys. Rep. **357**, 215 (2002).
[6] J. Wrkich, D Mathews, I. Kanik, S. Trajmar, and M. A. Khakoo, J. Phys. B **35**, 4695 (2002).
[7] G. Herzberg, *Molecular Spectra and Molecular Structure I. Spectra of Diatomic Molecules*, Edition 2 (Van Nostrand, New York, 1950).
[8] A. Lofthus and P. H. Krupenie, J. Phys. Chem. Ref. Data, **6**, 115 (1977).
[9] E. W. McDaniel, *Atomic Collisions Electron and Photon Projectiles* (Wiley, New York, 1989), p. 290.
[10] J. Mazeau, F. Gresteau, R. I. Hall, G. Joyez, and J. Reinhardt, J. Phys. B **6**, 862 (1973).
[11] T. G. Finn and J. P. Doering, J. Chem. Phys. **64**, 4490 (1976).
[12] F. M. Aarts and F. J. de Heer, Chem. Phys. Lett. **4**, 116 (1969).
[13] D. C. Cartwright, S. Trajmar, A. Chutjian, and W. Williams, Phys. Rev. A **16**, 1013 (1977).
[14] D. C. Cartwright, S. Trajmar, A. Chutjian, and W. Williams, Phys. Rev. A **16**, 1041 (1977).
[15] S. K. Srivastava, A. Chutjian, and S Trajmar, J. Chem. Phys. **64**, 1340 (1976).
[16] J. W. McConkey and J. A. Preston, J. Phys. B **8** 63 (1975).
[17] D. F. Register, S. Trajmar, and S. K. Srivastava, Phys. Rev. A **21**, 1134 (1980).
[18] P. Zetner and S. Trajmar, in *Proceedings of the XV ICPEAC*, edited by J. Geddes *et al.* (Brighton, U.K., 1987). Data tabulated in Ref. [5].
[19] J. C. Nickel, P. W. Zetner, G. Shen, and S. Trajmar, J. Phys. E **22**, 730 (1989).
[20] M. Allan, J. Electron Spectrosc. Relat. Phenom. **48**, 219 (1989).
[21] G. Poparić, M. Vićić, and D. S. Belić, Chem. Phys. **240**, 283 (1999).
[22] D. C. Cartwright, S. Trajmar, W. Williams, and D. L. Huestis, Phys. Rev. Lett. **27**, 704 (1971).
[23] W. A. Goddard III, D. L. Huestis, D. C. Cartwright, and S. Trajmar, Chem. Phys. Lett. **11**, 329 (1971).
[24] L. R. LeClair and S. Trajmar, J. Phys. B **29**, 5543 (1996).
[25] L. R. Le Clair, S. Trajmar, M. A. Khakoo, and J. C. Nickel, Rev. Sci. Instrum. **67**, 1753 (1996).
[26] J. M. Ajello and D. E. Shemansky, J. Geophys. Res. **90**, 9845 (1985); private communication.
[27] W. L. Borst, Phys. Rev. A **5**, 648 (1972).
[28] N. J. Mason and W. R. Newell, J. Phys. B **20**, 3913 (1987).
[29] L. A. Collins and B. I. Scheider, in *Electronic and Atomic Collisions*, edited by H. B. Gilbody, W. R. Newell, F. H. Read, and A. C. H. Smith (Elsevier Science, New York, 1988), pp. 57–72.
[30] D. L. Azevedo and M. A. P. Lima, Phys. Rev. A **63**, 062703 (2001); R. F. da Costa, F. J. da Paixão, and M. A. P. Lima, J. Phys. B **37**, L129 (2004).
[31] C. J. Gillan, C. J. Noble, and P. G. Burke, J. Phys. B **23**, L407 (1990).
[32] C. J. Gillan, J. Tennyson, B. M. McLaughlin, and P. G. Burke, J. Phys. B **29**, 1531 (1996).
[33] M. A. Khakoo, C. E. Beckmann, S. Trajmar, and G. Csanak, J. Phys. B **27**, 3159 (1994).
[34] M. Hughes, K. E. James, J. G. Childers, and M. A. Khakoo, Meas. Sci. Technol. **14**, 841 (2003).
[35] P. Johnson, I. Kanik, M. A. Khakoo, J. W. McConkey, and S. Tayal, J. Phys. B **36**, 4289 (2003).
[36] J. G. Childers, K. James, Jr., Igor Bray, M. Baertschy, and M. A. Khakoo, Phys. Rev. A **69**, 022709 (2004).
[37] W. Benesch, J. T. Vanderslice, S. G. Tilford, and P. G. Wilkinson, Astrophys. J. **142**, 1227 (1965).
[38] Y. Tanaka, M. Ogawa, and A. S. Jursa, J. Chem. Phys. **40**, 3690 (1964).
[39] F. R. Gilmore, R. R. Laher, P. J. Espy, J. Phys. Chem. Ref. Data **21**, 1005 (1992); R. Laher (private communication).
[40] T. W. Shyn and G. R. Carignan, Phys. Rev. A **22**, 923 (1980).
[41] J. C. Nickel, C. Mott, I. Kanik, and D. C. McCollum, J. Phys. B **21**, 1867 (1988).
[42] M. Gote and H. Ehrhardt, J. Phys. B **28**, 3957 (1995).
[43] G. H. Dunn, Phys. Rev. Lett. **8**, 62 (1962).
[44] E. N. Lassettre, Can. J. Chem. **47**, 1733 (1969).
[45] K. Jung, Th. Antoni, R. Muller, K.-H. Kochem, and H. Ehrhardt, J. Phys. B **15**, 3535 (1982).
[46] J. Geiger and B. Schroder, J. Chem. Phys. **50**, 7 (1969).